Accepted Manuscript

Structural and Crystal Chemical Properties of Alkali Rare-earth Double Phosphates

J.Matt Farmer, L.A. Boatner, Bryan C. Chakoumakos, Claudia J. Rawn, Jim Richardson

PII: S0925-8388(15)31100-2

DOI: 10.1016/j.jallcom.2015.09.124

Reference: JALCOM 35399

To appear in: *Journal of Alloys and Compounds*

Received Date: 30 July 2015

Revised Date: 11 September 2015

Accepted Date: 14 September 2015

Please cite this article as: J.M. Farmer, L.A. Boatner, B.C. Chakoumakos, C.J. Rawn, J. Richardson, Structural and Crystal Chemical Properties of Alkali Rare-earth Double Phosphates, *Journal of Alloys and Compounds* (2015), doi: 10.1016/j.jallcom.2015.09.124.

This is a PDF file of an unedited manuscript that has been accepted for publication. As a service to our customers we are providing this early version of the manuscript. The manuscript will undergo copyediting, typesetting, and review of the resulting proof before it is published in its final form. Please note that during the production process errors may be discovered which could affect the content, and all legal disclaimers that apply to the journal pertain.

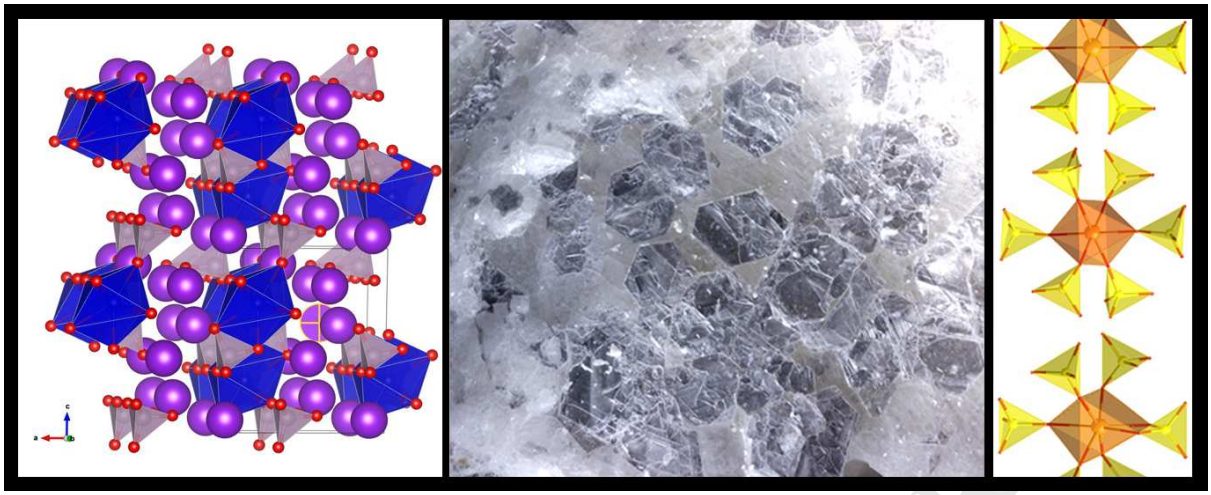

ACCEPTED MANUSCRIPT

ACCEPTED MANUSCRIPT

Structural and Crystal Chemical Properties of Alkali Rare-earth Double Phosphates

J. Matt Farmer[1], L. A. Boatner[1,2a], Bryan C. Chakoumakos[3], and Claudia J. Rawn[1]

[1]Materials Science and Technology Division

[2]ORNL Center for Radiation Detection Materials and Systems

[3]Quantum Condensed Matter Division

Oak Ridge National Laboratory, Oak Ridge, TN 37831- 6044, USA

and

Jim Richardson*

Argonne National Laboratory, Argonne, IL 60439, USA

"*Notice: "This manuscript has been authored by UT-Battelle, LLC under Contract No. DE-AC05-00OR22725 with the U.S. Department of Energy. The United States Government retains and the publisher, by accepting the article for publication, acknowledges that the United States Government retains a non-exclusive, paid-up, irrevocable, world-wide license to publish or reproduce the published form of this manuscript, or allow others to do so, for United States Government purposes.*

a)Author to whom correspondence should be addressed:

L. A. Boatner (boatnerla@ornl.gov)

Oak Ridge National Laboratory

1 Bethel Valley Road

Oak Ridge, TN 37831

*Deceased

ACCEPTED MANUSCRIPT

Abstract

When appropriately activated, alkali rare-earth double phosphates of the form: $M_3RE(PO_4)_2$ (where M denotes an alkali metal and RE represents either a rare-earth element or Y or Sc) are of interest for use as inorganic scintillators for radiation detection at relatively long optical emission wavelengths. These compounds exhibit layered crystal structures whose symmetry properties depend on the relative sizes of the rare earth and alkali-metal cations. Single-crystal X-ray and powder neutron diffraction methods were used here to refine the structures of the series of rare-earth double phosphate compounds: $K_3RE(PO_4)_2$ with RE = Lu, Yb, Er, Ho, Dy, Gd, Nd, Ce, plus Y and Sc - as well as the compounds: $A_3Lu(PO_4)_2$, with A = Rb, and Cs. The double phosphate $K_3Lu(PO_4)_2$ was reported and structurally refined previously, and it exhibited two lower-temperature phases. The compound $K_3Yb(PO_4)_2$ reported here also exhibits a new second phase that occurs at T = 120°C with a transformation to hexagonal *P*-3 space group symmetry and a Yb-ion coordination number reduction from seven to six. This latter result was confirmed using EXAFS. Comprehensive structural data and structural systematics are reported here for a number of alkali rare-earth double phosphates. Additionally, single-crystal growth methods for the preparation of large single crystals of these compounds are described, and the thermal expansion properties of the present series of alkali rare-earth double phosphates, as determined by both X-ray and neutron diffraction methods, are presented. These data represent a structural and thermal characteristics basis for continuing research on the use of alkali rare-earth double phosphates as scintillators for radiation detection - as well as for future studies of the fundamental phase properties of these compounds at elevated pressures.

Key Words: rare earth alloys and compounds

ACCEPTED MANUSCRIPT

1. Introduction

Rare-earth phosphates in both the orthophosphate and alkali rare-earth double phosphate forms continue to be studied as single-crystal hosts for use as inorganic scintillators for radiation detection applications[1-12]. In particular, alkali double phosphates of rare-earth elements with the general formula $M_3RE(PO_4)_2$ (where M denotes an alkali metal and RE represents either a rare-earth element or Y or Sc) are candidate materials for use as gamma-ray scintillators. When activated with Ce^{3+}, these materials exhibit relatively high scintillation light yields, rapid decay times, relatively short attenuation lengths, and the potential for growth in large single-crystal forms. Additionally, since they scintillate in the wavelength region above ~450 nm, they are amenable for use in combination with silicon solid-state detectors instead of photomultiplier tubes. Also, when isotopically enriched ^6Li is substituted on the alkali metal ion site, the Ce^{3+}-activated compounds are of interest for applications as scintillators for neutron detection[11].

The structures of these compounds are closely related to the glaserite structure. Glaserite (or aphthitalite) is an anhydrous sulfate $(K,Na)_3Na(SO_4)_2$, found in volcanic fumaroles. The glaserite structure and its derivatives are common in the $A_2X_2O_4$ molybdates, tungstates, phosphates, and silicates.[13-17] The $M_3RE(XO_4)_2$ compounds with M = Rb, K, and RE = a rare earth, Sc, or Y, and X = P, As, or V were reported previously by Melnikov et al.[18,19] who prepared the double phosphate compounds by a reaction of the orthophosphate $REPO_4$ with M_2CO_3 in the presence of H_3PO_4 at 450-700°C for 50-150 h. This process resulted in powder $M_3RE(PO_4)_2$ compounds based on the $K_3Na(PO_4)_2$ glaserite structure[20,21] - consisting of an (NaO_6) trigonal antiprism (an octahedron) that shares its six corners with (PO_4) tetrahedra. These compounds were initially characterized using powder XRD methods[20]. Melnikov et al.[19] categorized the synthesized phases into three groups: hexagonal (isostructural to glaserite) and

two separate monoclinic structures. The Rb double-salts $Rb_3RE(XO_4)_2$ (where RE = a rare earth, Sc, or Y, and X = P, As, V) were also reported to be isostructural with glaserite along with the ternary cesium rubidium rare-earth phosphates: $Rb_2CsRE(PO_4)_2$ with RE = Sm to Lu, Y. The observation that the mixed-alkali compound $K_2CsYb(PO_4)_2$ also crystallizes in the glaserite structure was previously reported by Rghioui[22].

Mixed phosphate/vanadate $K_3Y(PO_4)_x(VO_4)_{2-x}$ solid solutions occur in two structural types[23]: First there are compounds that are based on monoclinic $K_3Y(PO_4)_2$ – a material with an arcanite-like structure, and second, there are materials based on hexagonal $K_3Y(VO_4)_3$ - a compound with the glaserite structure. When Y^{3+} is substituted by Eu^{3+}, the extent of solid solution with the monoclinic $K_3Y(PO_4)_2$ structure is increased. The compounds $K_3Y(VO_4)_2$ and $K_3Y_{1-y}Eu_y(PO_4)_x(VO_4)_{2-x}$ have also been synthesized. Additionally, Komissarova et al.[24] have reported the occurrence of solid solutions of $K_3RE(PO_4)_2$-$K_3RE(VO_4)_2$, where RE = Sc, Y, La, Eu, Gd, and Yb. Furthermore, their work demonstrated that continuous solid solutions exist for the rare-earth cations Sc, La, Eu, and Gd - but for the case of Y and Yb, only limited solid solutions are obtained.

The early data on both the thermodynamic chemical stability and structural phase transformations for the alkali rare-earth double phosphate compounds were incomplete and fragmentary. Recently, however, the formation and phase-transition enthalpies were determined using oxide-melt solution calorimetry and reported by Ushakov et al.[25] for the potassium and rare-earth double phosphates. The structure type for these compounds changes from glaserite to monoclinic - as in the case of the lutetium double phosphates with K and Rb with the glaserite-type structure.[25] The cumulative thermochemical data for these materials suggested that, for the $M_3RE(XO_4)_2$ compounds, increasing the size of either the M cation (e.g., from K to Rb) or of the

ACCEPTED MANUSCRIPT

XO_4 tetrahedra (e.g., from $[PO_4]$ to $[VO_4]$) stabilizes the hexagonal glaserite structure over the monoclinic structure.

Some preliminary selected structural results for the alkali rare-earth double phosphates were given previously in the work of Ushakov et al.[25] for the purpose of interpreting the thermodynamic calorimetry results. In the current work, we present the details of the single-crystal growth, single-crystal structural analysis (using both neutron and X-ray diffraction methods), the observation of new phase transitions, and data on the thermo-mechanical properties of an extended series of rare-earth alkali double phosphates. Our previous investigations[26] have established that, in particular, the compound $K_3Lu(PO_4)_2$ undergoes a structural phase change with increasing temperature and that this phase transition is highly hysteretic. Other alkali rare earth double phosphate transformation studies have previously been limited to a phase transition (i.e., hexagonal → monoclinic) that is produced by a pressure effect[27], and one prior study used infrared spectroscopy to investigate the existence of both the hexagonal and monoclinic alkali RE double phosphate phases[28]. Precise and comprehensive structural and temperature-related data of the type obtained in the present work are particularly important for continuing investigations of the effects of structural changes on the scintillation properties of these materials and of the effects of heavy-particle radiation damage in the $K_3RE(PO_4)_2$ series of compounds.

2. Ideal Glaserite Structure

The crystal chemistry of glaserite-related structures has been studied extensively[29]. Moore[16] introduced a *bracelet* and *pinwheel* description for glaserite-like sulfates. Adopting this approach for the glaserite-type alkali RE double phosphates, the pinwheel or structural sub-unit is formed by the $[REO_6]$ octahedron that shares its six corners with $[PO_4]$ tetrahedra that

alternate “up” and “down”. The pinwheels are linked through [PO_4] tetrahedra to form layers with alkali atoms located between the layers. The changes in the pinwheel for the structures under consideration are shown in Figure 1. The glaserite structure as described by Moore[16] consists of an (NaO_6) trigonal antiprism (octahedron) that shares its six corners with (SO_4) tetrahedra. The six tetrahedra are alternating “up” and “down” groups around the central ion, type (3 + 3)*c*’. The $K_3Lu(PO_4)_2$ alkali RE double structure has a slightly distorted glaserite structure as shown in Figure 1. The phosphate groups rotate, and thus, decrease the glaserite structure symmetry from *P*-3*m*1 (No.167) to *P*-3 (No. 147). The monoclinc distortion of the glaserite structure appears to resemble the arcanite (4 + 2)*a*’ structure. The bidentate phosphate group, the top phosphate group in Figure 1, apparently flips directions to a “d” group.

In this work, the compound $Rb_3Lu(PO_4)_2$ (*P*-3*m*1) was found to have the most symmetric pinwheel structure. $K_3Sc(PO_4)_2$ and $K_3Lu(PO_4)_2$ are also hexagonal, but one [PO_4] tetrahedron is rotated in such a way that it reduces the symmetry to *P*-3. In the structures of all of the other $K_3RE(PO_4)_2$ compounds investigated here, one of the six [PO_4] tetrahedra, comprising each pinwheel, shares an edge with the RE polyhedra. This increases the RE coordination number to seven and reduces the symmetry to monoclinic ($P2_1/m$). This monoclinc distortion of the glaserite structure resembles the arcanite (K_2SO_4) structure, and the alkali ions for the layered structure are located within channels of the unit cell as illustrated in Figure 2.

3. Experimental

A. Crystal Growth

Single-crystals of $K_3RE(PO_4)_2$ (where RE = Lu – Ce [except for Pm], Y and Sc) were grown from a high-temperature solution using 12 wt% of the respective 99.99%-pure rare-earth oxide (RE_2O_3) combined with 88 wt% of potassium pyrophosphate ($K_4P_2O_7$)[26]. The mixture was

ACCEPTED MANUSCRIPT

heated in air to 1235°C in a platinum crucible and held at this temperature for 4 h. The crucible was then slowly cooled to 900°C at 1°C/h followed by rapid cooling to room temperature. The balanced reaction is: $RE_2O_3 + 3\ K_4P_2O_7 \rightarrow 2\ K_3RE(PO_4)_2 + 2\ K_3PO_4$ ($3\ K_2O + P_2O_5$). Figure 3 shows a photograph of single crystals of $K_3Yb(PO_4)_2$ still embedded in the solidified flux, while Figure 4 shows clear single crystal plates of $K_3Lu(PO_4)_2$ that were cleaved from a larger crystal after removal from the growth flux. The relative size of the $K_3Lu(PO_4)_2$ crystals was usually approximately ten times that of the $K_3Yb(PO_4)_2$ crystals, and $K_3Lu(PO_4)_2$ crystals would sometimes grow completely across the cross section of the 50 ml Pt crucible.

The remaining rare-earth and yttrium double phosphates [$K_3RE(PO_4)_2$ where RE = Tm – Ce, and Y] have growth habit morphologies that are similar to the potassium ytterbium double phosphate as shown in the photographs in Fig. 3. Single-crystals of the rare-earth double phosphates with alkali ions other than potassium were also grown from a high-temperature solution using a rubidium or cesium pyrophosphate ($Rb_4P_2O_7$ or $Cs_4P_2O_7$) flux with the addition of 12 wt.% of the corresponding rare-earth oxide and using the same thermal conditions described above for the growth of the potassium rare-earth double phosphates .

B. Single-Crystal X-ray Diffraction Collection Methods

The data collection methods for the structural refinement of the alkali rare-earth double phosphates have been described in detail previously[26] in our article on the properties of the different phases of the single crystal $K_3Lu(PO_4)_2$ compound. For the series of $K_3RE(PO_4)_2$ compounds (where RE = Tm – Ce [except Pm], and Y) investigated here, the subject plate-like single-crystals were mounted on an Enraf-Nonius CAD4-F auto-diffractometer, and data were collected at 19°C using MoK_α radiation (λ_{mean} = 0.71073Å). The final lattice constants were obtained at high θ angles, > 20°. Intensities were measured in the ω–2θ mode at a varied scan

rate of 0.56 - 5.l7° min^{-1}. Intensity variations selected from different zones of reciprocal space were negligible during the data collection (<1.0%). Intensity measurements were corrected for Lorentz and polarization factors and by applying either a numerical absorption correction based on six crystal-face measurements or a semi-empirical absorption correction based on azimuthal scans of ψ-data[30]. Systematic absences established that the compounds crystallize in the space group $P2_1/m$ (0k0): k = 2n, and the absence of additional symmetry was confirmed by utilizing the program MISSYM. The clear single-crystals of $Rb_3Lu(PO_4)_2$ and $Rb_3Er(PO_4)_2$ were also examined using the Enraf-Nonius CAD4-F auto-diffractometer, and initial cell parameters were obtained from least-squares refinements of twenty-five accurately centered matrix reflections. Intensities for both of these compounds were also measured in the ω-2θ scan mode in the 2θ range 3.0° - 50.0° (h: -6 → 6, k: 0 → 6, l: 0 → 9), and the data were corrected for Lorentz and polarization factors along with a semi-empirical correction.

C. Single-Crystal X-Ray Diffraction Structural Refinement Methods

Refinements of the compounds $K_3RE(PO_4)_2$ where RE = Tm, Ho, Nd, Pr, Ce, and La plus $Rb_3Lu(PO_4)_2$ and $Rb_3Er(PO_4)_2$ were made by the full-matrix least-squares method on all F^2 data, using the SHELX-97 program.[30] The structural parameters of the various $K_3RE(PO_4)_2$ (where RE = Tm, Ho, Nd, Pr, Ce, and La), as obtained from refinements of the single-crystal X-ray diffraction data, are summarized in Table 1. Final difference Fourier maps indicate some residual density near the rare-earth positions. The Atomic coordinates and equivalent isotropic thermal coefficients (Å x 10^3) for the example of $K_3Tm(PO_4)_2$ are shown in Table 2. The other atomic coordinates for the Ho, Nd, Pr, Ce, and La complexes are listed in Appendix A. All were refined anisotropically. The anisotropic atomic displacement parameters are shown in Appendix

B. Intensity data for $K_3RE(PO_4)_2$ (where RE = Er, Dy, Sm, or Y) were not refinable due to crystal degradation during the centering procedure. Previously studies have revealed the hygroscopic nature of many of the double phosphates.[26] The water in-take, therefore, may contribute to the peak broadening; however multiple mounting techniques (mounting in a dry box in a capillary tube and at low temperature) all failed to produce good refinable data. Therefore, the final cell parameters for $K_3RE(PO_4)_2$ (where RE = Er, Dy, Sm, and Y) will only be used here for comparison with the other double phosphates.

The relevant crystallographic data for $Rb_3Lu(PO_4)_2$, $Rb_3Er(PO_4)_2$, and $K_3Sc(PO_4)_2$ are listed in Table 3. Residual density near the positions of the lutetium ions was found from the final difference Fourier maps. Elsewhere, the residual map was virtually featureless revealing only random fluctuating backgrounds. The atomic coordinates and equivalent isotropic atomic displacement parameters for $Rb_3Lu(PO_4)_2$ are listed in Table 4, and the atomic coordinates for $Rb_3Er(PO_4)_2$, and $K_3Sc(PO_4)_2$ are listed in Appendix A. All of the anisotropic atomic displacement parameters are shown in Appendix B.

D. High-Temperature X-Ray Diffraction

High-temperature X-ray diffraction (HTXRD) measurements for $K_3Yb(PO_4)_2$ were made using a Scintag PAD V vertical θ/θ goniometer equipped with a Buehler HDK-2 diffraction furnace. The diffractometer utilized Cu K_α radiation (45 kV and 40 mA) and a Si(Li) Peltier-cooled solid-state detector. The single-crystals were crushed into a powder for these analyses. Data were collected as step scans with a step size of 0.02° 2θ and a count time of 1 s/step between 10° and 60° 2θ. The sample temperature was monitored with a Pt/Pt-10% Rh thermocouple spot-welded to the Pt-30% Rh heater strip on which a thin layer of the double phosphate powders was dispersed. Some high-temperature readings (>900˚C) of the

thermocouple were checked with an optical pyrometer (Pyrometer Instrument Co., Inc., Bergenfield, NJ, model 95) and were within 1% of the set temperature. The $K_3Yb(PO_4)_2$ complex data was collected up to 800˚C and then, by decreasing the temperature in 50˚C increments, down to 20˚C - see Figure 5. All of the data were analyzed using the JADE 6.0 program[31]. The starting values for the $K_3Yb(PO_4)_2$ refinements were obtained from the single-crystal X-ray diffraction analysis. The (111) and (200) diffraction peaks originating from the Pt/Rh heater strip at approximately 40.5° and 47.1° 2θ, respectively, were excluded from the refinements.

For $K_3Gd(PO_4)_2$ and $K_3Y(PO_4)_2$, powder X-ray diffraction experiments (HTXRD) were performed at both room and high temperatures using an INEL diffractometer equipped with a position-sensitive detector (CPS120) and a Ge (111) incident-beam monochromator using CuK_α radiation. The HTXRD measurements were performed in the case of the $K_3Y(PO_4)_2$ and $K_3Gd(PO_4)_2$ samples in static air at 100, 770, and 1000°C (Figure 10). The samples were heated to the desired temperature at 10°C per min, and XRD patterns were collected for 2 h after a 0.5 h equilibration time. A fluorescence filter was used to increase the signal-to-noise ratio in the $K_3Gd(PO_4)_2$ XRD patterns. Figure 6 indicates that the high-temperature phases of $K_3Y(PO_4)_2$ and $K_3Gd(PO_4)_2$ are isostructural or closely related to the glaserite structure in which $K_3Sc(PO_4)_2$ and $K_3Lu(PO_4)_2$ exist at room temperature. The peak shift towards lower 2-theta values indicates an increase in the cell parameters of the high-temperature phases of $K_3Y(PO_4)_2$ and $K_3Gd(PO_4)_2$ as compared with $K_3Sc(PO_4)_2$.

E. Neutron Powder Diffraction

Neutron powder diffraction (NPD) measurements were made for the $K_3Yb(PO_4)_2$ compound using the General Purpose Powder Diffractometer (GPPD) at Argonne National

ACCEPTED MANUSCRIPT

Laboratory's Intense Pulse Neutron Source, that utilizes the time-of-flight (TOF) method. Single-crystals of $K_3Yb(PO_4)_2$ were crushed into powder and placed into cylindrical V cans and diffraction data were collected at a scattering angle of 90° to achieve a resolution of $\Delta d/d$ = 0.49%. The sample was heated at 100˚C /h using a Howe vacuum furnace and held at the desired temperature for 30 min. for thermal stabilization before the data collection. The sample temperature, monitored by thermocouples above and below the sample, was controlled at a selected temperature to within 10˚C in all runs. The data-collection times at 20 and 200˚C were 8 h, and 1 h periods were used for T = 300 to 800˚C. A statistical summary of the results for $K_3Yb(PO_4)_2$ at 20 and 200˚C is listed in Table 5. These data were analyzed by the Rietveld refinement technique using the Generalized Structural Analysis System (GSAS) computer code[33]. The background was defined by a cosine Fourier series with four terms refined simultaneously with the other profile and structural parameters. The graphical fits of the Rietveld refinements for $K_3Yb(PO_4)_2$ at 20 and 200˚C are shown in Figures 7a and 7b, respectively.

III. Results and Discussion

A. Single-Crystal X-Ray Diffraction Studies

The $K_3RE(PO_4)_2$ (RE = Yb – Ce, La, and Y) compounds crystallize in the monoclinic space group $P2_1/m$ (No. 11), Z = 2, where the atomic positions for RE, P, and K occupy 2*e* sites (*x*,1/4,*z*), and the oxygen atoms are distributed between the 2*e* and the general 4*f* positions. The basic structural units are isolated PO_4 tetrahedra and REO_7 polyhedra. The RE ion is seven-fold coordinated with a slightly distorted capped trigonal prism (CTP) geometry. The REO_7 polyhedra each connect six PO_4 tetrahedra to form $RE(PO_4)_2^{-3}$ layered sheets perpendicular to

[100]. One of the six PO_4 groups connected to the REO_7 polyhedra is bidentated. The potassium ions are positioned within channels of the unit cell between the polymeric layers, see Figure 8a.

A summary of the room-temperature SXRD indexing of $A_3RE(PO_4)_2$, where RE = a rare-earth ion and A = K or Rb, is shown in Table 6. The changes in the volume per unit cell across the $K_3RE(PO_4)_2$ series are shown in Figure 9. For the monoclinic $K_3RE(PO_4)_2$ compounds, the volume increases nearly linearly as the rare-earth crystal radius increases and, accordingly, the densities decrease across the series, see Table 6. The geometry about the RE ion is seven-coordinated forming a slightly distorted capped trigonal prism arrangement (CTP, with C_{2v} symmetry) The 7-coordinated RE atoms are linked together by slightly distorted tetrahedral phosphate groups, Figure 8a. $K_3RE(PO_4)_2$ bond distances (Å) and phosphate angles (˚) (where RE = Lu, Yb, Tm, Ho, Nd, Pr, Ce, and La) are found in Tables 7 and 8, respectively. The unit cell parameters of $K_3Tm(PO_4)_2$ are a = 7.368(1), b = 5.585(1), c = 9.311(1) Å and β = 90.81° and the average Tm-O bond length is 2.36 Å. The mean P-O distance is 1.54 Å which is in good agreement with the sum of the radii of P^{5+} and O^{2-} (1.53 Å) as obtained from the work of Shannon.[32] The Tm analog bond angle, O(1)-P-O(2) , for the bidentate phosphate group is 105.4(7)˚, and the O(1)-P-O(2) angle for the rest of the rare-earth series is less than the optimal tetrahedral angle of 109.5˚.

The bond distances for the $K_3RE(PO_4)_2$ compounds (where RE = Lu, Yb, Tm, Ho, Nd, Pr,Ce, and La) are shown in Table 7. All of the RE-O bond distances, except the RE-O(2), increase in a near-linear relationship with increasing RE^{+3} crystal radius. However, the RE-O(2) bond distances indicate a non-linear relationship with respect to the crystal radius. This may be due to the unstable nature of the bidentated phosphate group. The degree of asymmetry in the bidentated phosphate group is determined by the difference between the RE-O(1) and RE-O(2)

bond distance. A large degree of asymmetry is indicated by a large difference between the two bond distances, see Table 9. Figure 9 shows the RE-O(1) – RE-O(2) bond difference (Å) vs. RE^{+3} crystal radius. The largest asymmetry is indicated for the Lu, Yb, and Tm complexes. This indicates an unstable measure for the transformation from seven to six coordination, in which the R-O(2) distance moves beyond a bonding distance with the central RE ion.

$Rb_3Lu(PO_4)_2$ and $Rb_3Er(PO_4)_2$ crystallize in the *P*-3*m*1 space group (No.164), Z = 1, and the compounds adopt the idealized glaserite structure, see Figure 1. The structural sub-unit is formed by the [REO_6] octahedron that shares its six corners with [PO_4] tetrahedra that alternate "up" and "down". The compound exhibits a layered crystal structure, with the Rb ions located within channels of the unit cell. The atomic layers are in the sequence: rare-earth, phosphate – rubidium, rubidium, rubidium - phosphate. The density of $Rb_3Lu(PO_4)_2$ and $Rb_3Er(PO_4)_2$ was determined to be 4.676 and 4.559 Mg/m^3, respectively. A preliminary analysis of the $Cs_3Lu(PO_4)_2$ compound indicates a similar layer structure with an increased density of 4.885 Mg/m^3. The bond distances and angles for $Rb_3Lu(PO_4)_2$ and $Rb_3Er(PO_4)_2$ are shown in Table 10. The Lu-O(1) bond distance of 2.195(6) Å is slightly smaller than the Er-O(1) bond distance of 2.236(7) Å.

B. High Temperature X-Ray Diffraction and Neutron Powder Diffraction of $K_3Yb(PO_4)_2$

The $K_3Yb(PO_4)_2$ complex crystallizes at room temperature in the monoclinic $P2_1/m$ space group. The K ions are located within channels of the unit cell. The Yb ion is seven-coordinated to six tetrahedrally arranged phosphate groups, one of which is bidentate (Figure 1). A high-temperature X-ray diffraction (HTXRD) analysis has indicated that $K_3Yb(PO_4)_2$ has a high-temperature phase transition at 200˚C. The HTXRD indicates that this phase transition is

ACCEPTED MANUSCRIPT

reversible with a large thermal hysteresis. Phase transitions for $K_3Tm(PO_4)_2$ and $K_3Er(PO_4)_2$ have also been observed that are similar to those observed for the Yb complex using HTXRD.

A time-of-flight neutron powder diffraction (TOF-NPD) study indicated that $K_3Yb(PO_4)_2$ has two polymorphs. Using the furnace capabilities of the powder diffraction (GPPD) system, two phases for $K_3Yb(PO_4)_2$ were studied. A Rietveld refinement at room temperature (Figure 7a) confirms that the Yb ion is seven-fold coordinated, and includes one bidentate phosphate group and five unidentate phosphate groups, see Figure 10a. A Rietveld refinement at 200°C (Figure 7b) indicates a loss of the bidentation of the phosphate group, leaving a coordination number of six around the Yb ion and a symmetry increase to the hexagonal, *P*–3 space group, see Figure 10b. This new high-temperature structure for $K_3Yb(PO_4)_2$ is isostructural with the room-temperature structure of $K_3Lu(PO_4)_2$ as shown in Figure 8b.

Neutron powder data can be used to study more precisely the nuclear positions through the structural phases - specifically, to study the oxygen shift through the sites surrounded by high-electron-dense atoms. TOF-NPD data were collected from T = 300 to 800°C at 100°C intervals for 1 h to study the anisotropic thermal expansion. The data refinements indicate a significant difference in the expansion of the *c*-axis as compared to the *a*-axis. Upon cooling, a kinetic study was performed on $K_3Yb(PO_4)_2$ by collecting data sets as the furnace cooled (~ 40 °C) at 30 min intervals. This was a unique opportunity to study the transformation percentage of hexagonal to monoclinic phases. A refinement of the polyphase sample containing the lower-temperature hexagonal (*P*-3) phase that transforms into the room-temperature monoclinic ($P2_1/m$) phase was analyzed over a 3 h period. During this time, the percentage of $P2_1/m$ shows a linear decrease of the transformation to the monoclinic structure, which indicates a first-order transition.

ACCEPTED MANUSCRIPT

338

339 **C. Thermal Expansion using High-Temperature Neutron and X-ray Powder Diffraction**

340 The thermal expansion of $K_3Yb(PO_4)_2$ was determined using both high-temperature X-
341 ray and time-of-flight neutron powder diffraction methods. Since this compound crystallizes in a
342 monoclinic space group ($P2_1/m$) at room temperature, the $K_3Yb(PO_4)_2$ sample was heated past
343 the hexagonal phase transition to T = 200˚C. The resulting lattice parameters at this temperature
344 served as the initial a_0, c_0, and $v_0^{1/3}$ parameters. The $\Delta L/L_0$ vs. temperature results for the X-ray
345 and neutron data for $K_3Yb(PO_4)_2$ are shown in Figure 11. A linear fit was used to determine the
346 coefficient of thermal expansion. The thermal expansion of $K_3Yb(PO_4)$ calculated using both X-
347 ray and Neutron powder diffraction is shown in Table 11.

348 The high-temperature hexagonal phase of $K_3Yb(PO_4)_2$ and $K_3Lu(PO_4)_2$ has a large
349 thermal expansion anisotropy in the c-drection (α_c/α_a = 7.27 and 0.3˚C^{-1}, respectively, as
350 etermined using HTXRD). It should be noted that anistropies in both the elasticity and thermal
351 conductivity of a number of monazite-type rare-earth orthophosphates have been predicted
352 previously from first-principals calculations[34]. It is anticipated that similar srudies of the alkai
353 rare-earth double phosphates investigated here would yield similar results for their elasticity and
354 thernal conductivity characteristics. The coefficients of thermal expansion for $K_3Yb(PO_4)_2$ as
355 determined by both the neutron and X-ray measurement methods are in good agreement.

356

357 **IV. Conclusion**

358

359 $K_3RE(PO_4)_2$ crystals with RE = Sc, Y, Lu, Yb, Er, Ho, Dy, Gd, Nd, Ce and for
360 $A_3Lu(PO_4)_2$, with A = K, Rb, and Cs were grown from a $A_4P_2O_7/RE_2O_3$ flux. The predominant
361 room-temperature crystal structure for the RE series is $P2_1/m$ (La – Yb), in which the RE atom is

ACCEPTED MANUSCRIPT

ACCEPTED MANUSCRIPT

coordinated to 7 oxygen atoms, and this coordination polyhedron becomes more regular with increasing size of the RE. Neutron powder diffraction and high-temperature X-ray diffraction studies have confirmed the existence of two phases for $K_3Yb(PO_4)_2$. The high-temperature phase of $K_3Yb(PO_4)_2$ is isostructural with the room temperature structure of $K_3Lu(PO_4)_2$ (Hexagonal *P*-3, C.N. = 6) - a compound that was previously found to exhibit three distinct phases on cooling from room temperature[26]. The rare-earth coordination number for $K_3Yb(PO_4)_2$ decreases from seven to six during the high-temperature transition. These $K_3Yb(PO_4)_2$ phase changes are structurally reversible, but a large hysteresis is observed on cooling.

Acknowledgements

Research at the Oak Ridge National Laboratory was sponsored in part by the U.S. Department of Energy, Office of Science, Basic Energy Sciences (BES), Materials Sciences and Engineering Division and in part by the Office of Nonproliferation Research and Engineering in the Office of Defense Nuclear Nonproliferation in the National Nuclear Security Administration (NNSA). LAB was supported by the NNSA, and JMF and CJR were supported by the U.S. DOE/BES. BCC was supported by the U.S. DOE Scientific User Facilities Division. The authors acknowledge with thanks the contributions of Sandra Salmen to the manuscript and graphic arts preparation.

ACCEPTED MANUSCRIPT

References

[1] A.J. Wojtowicz, A. Lempicki, D. Wisniewski, L.A. Boatner, Cerium-Doped Orthophosphate Scintillators, Mater. Res. Soc. Symp. P 348 (1994) 123-129.

[2] D. Wisniewski, S. Tavernier, P. Dorenbos, M. Wisniewska, A.J. Wojtowicz, P. Bruyndonckx, E. van Loef, C.W.E. van Eijk, L.A. Boatner, VUV scintillation of $LuPO_4$: Nd and YPO_4 : Nd, IEEE Trans. Nucl. Sci. 49 (2002) 937-940. Pii S0018-9499(02)06101-4, Doi:10.1109/Tns.2002.1039593.

[3] A. Lempicki, E. Berman, A.J. Wojtowicz, M. Balcerzyk, L.A. Boatner, Cerium-Doped Orthophosphates - New Promising Scintillators, IEEE Trans. Nucl. Sci. 40 (1993) 384-387. Doi:10.1109/23.256585.

[4] L.A. Boatner, L.A. Keefer, J.M. Farmer, D. Wisniewski, A.J. Wojtowicz, Cerium-activated rare-earth orthophosphate and double-phosphate scintillators for X- and gamma-ray detection, Proc. SPIE Vol. 5540, Hard X-ray and Gamma-Ray Detector Physics VI, Edited by Arnold Burger, Ralph B. James, and Larry A. Franks. (SPIE, Bellingham, WA,) 2004, 73-87. Doi: 10.1117/12.562220.

[5] D. Wisniewski, S. Tavernier, A.J. Wojtowicz, M. Wisniewska, P. Bruyndonckx, P. Dorenbos, E. Van Loef, C.W.E. Van Eijk, L.A. Boatner, $LuPO_4$:Nd and YPO_4:Nd—new promising VUV scintillation materials, Nucl. Instrum. Meth. A 486 (2002) 239-243. Doi:10.1016/S0168-9002(02)00709-X.

ACCEPTED MANUSCRIPT

[6] D. Wisniewski, A.J. Wojtowicz, W. Drozdowski, J.M. Farmer, L.A. Boatner, Scintillation and luminescence properties of Ce-activated $K_3Lu(PO_4)_2$, J. Alloy. Compd. 380 (2004) 191-195. Doi:10.1016/j.jallcom.2004.03.042.

[7] D.W. J. Wojtowicz, W. Drozdowski, J. M. Farmer, and L. A. Boatner, , Vacuum Ultraviolet Studies of a New Phosphor Material: $Rb_3Lu(PO_4)_2$:Ce, in: P.d.V. K. Neyts, D. Poelman (Ed.) Proceedings of the 2002 International Conference on the Science and Technology of Emissive Displays and Lighting, (Academia Press & Ghent University, Ghent 2002) 73-76.

[8] D. Wisniewski, A.J. Wojtowicz, W. Drozdowski, J.M. Farmer, L.A. Boatner, $Rb_3Lu(PO_4)_2$:Ce and $Cs_3Lu(PO_4)_2$:Ce – new promising scintillator materials, Cryst. Res. Technol. 38 (2003) 275-282. Doi:10.1002/crat.200310031.

[9] D. Wisniewski, A.J. Wojtowicz, L.A. Boatner, Properties of Ce-activated alkali-lutetium double phosphate scintillators, Radiat. Meas. 45 (2010) 400-402. Doi10.1016/j.radmeas.2009.10.019.

[10] J.S. Neal, L.A. Boatner, M. Spurrier, P. Szupryczynski, C.L. Melcher, Cerium-doped mixed-alkali rare-earth double-phosphate scintillators for X- and gamma-ray detection, Proc. SPIE 6319, Hard X-Ray and Gamma-Ray Detector Physics and Penetrating Radiation Systems VIII, (2006) 631907-631908. Doi:10.1117/12.683884.

[11] J.S. Neal, L.A. Boatner, M. Spurrier, P. Szupryczynski, C.L. Melcher, Cerium-doped mixed-alkali rare-earth double-phosphate scintillators for thermal neutron detection, Nucl. Instrum. Meth. A A579 (2007) 19-22. Doi:10.1016/j.nima.2007.04.005.

[12] D. Wisniewski, L.A. Boatner, Scintillation Properties and Time-Resolved Spectroscopy of a Novel Scintillator Material: Ce^{3+}-Activated $Li_3Lu(PO_4)_2$ Crystals, IEEE Trans. Nucl. Sci. 56 (2009) 3806-3818. Doi:10.1109/Tns.2009.2032290.

[13] B. Gossner, Neues Jahrb, Mineralogy, Geology and Paleontology 57 (1928) 89-116.

[14] M.A. Bredig, A new group of isomorphous compounds A_2X0_4, J. Amer. Chem. Soc. 63 (1941) 2533-2536. Doi:10.1021/ja01854a510.

[15] M.A. Bredig, Isomorphism and allotropy in compounds of the type A_2XO_4, J. Phys. Chem. 46 (1942) 747-764.

[16] P.B. Moore, Bracelets and Pinwheels: A Topological-Geometrical Approach to the Calcium Orthosilicate and Alkali Sulfate Structures, Am. Mineral. 58 (1973) 32-42.

[17] P.E. Tomaszewski, A. Pietraszko, M. Maczka, J. Hanuza, $CsAl(MoO_4)_2$, Acta Crystallogr. Sect. E: Struct. Rep. Online 58 (2002) I119-I120. Doi:10.1107/S1600536802020950.

[18] P. Melnikov, L. Komissarova, Double phosphates, arsenates and vanadates of rare-earth elements-scandium and yttrium with alkali-metals, Dokl. Akad. Nauk SSSR 256 (1981) 878-881.

[19] P. Melnikov, H. Quiroga, J.C. Heredero, L. Komissarova, Triple phosphates containing rubidium, cesium, and rare-earth cations, Dokl. Akad. Nauk SSSR 285 (1985) 1134-1136.

[20] P.P. Melnikov, V.A. Efremov, H. Quiroga, L.N. Komissarova, Triple phosphates containing rare earth and alkali metal cations, J. Less Common Met. 91 (1983) L21-L23. Doi:10.1016/0022-5088(83)90333-8.

ACCEPTED MANUSCRIPT

ACCEPTED MANUSCRIPT

446 [21] K. Okada, J. Ossaka, Structures of potassium sodium sulphate and tripotassium sodium
447 disulphate, Acta Crystallogr., Sect. B: Struct. Sci. 36 (1980) 919-921.
448 Doi:10.1107/S0567740880004852.

449 [22] L. Rghioui, L. El Ammari, L. Benarafa, J.P. Wignacourt, $K_2CsYb(PO_4)_2$, Acta Crystallogr.,
450 Sect. C: Cryst. Struct. Commun. 58 (2002) i90-i91. Doi:10.1107/S0108270102008107.

451 [23] A. N. Kirichenko, E. N. Otkidach, F. M. Spiridonov, V. F. Kharsika, L. N. Komissarova,
452 Zh. Neorg. Khim. 44 (7) (1999) 1061-1063.

453 [24] L. Komissarova, A. Bobylev, A. Kirichenko, G.Y. Pushkina, F. Spiridonov, Phase
454 formation in systems $K_3R(PO_4)_2$-$K_3R(VO_4)_2$ (R= Sc, Y, La, Eu, Gd, Yb), Zh. Neorg. Khim. 47
455 (2002) 684-688.

456 [25] S.V. Ushakov, K.B. Helean, A. Navrotsky, L.A. Boatner, Thermochemistry of rare-earth
457 orthophosphates, J. Mater. Res. 16 (2001) 2623-2633. Doi:10.1557/JMR.2001.0361.

458 [26] J.M. Farmer, L.A. Boatner, B.C. Chakoumakos, C.J. Rawn, D. Mandrus, R. Jin, J.C. Bryan,
459 Polymorphism, phase transitions, and thermal expansion of $K_3Lu(PO_4)_2$, J. Alloys Compd. 588
460 (2014) 182-189. Doi.: 10.1016/j.jallcom.2013.10.232.

461 [27] L. Rghioui, L. Benarafa, M. Saidi Idrissi, A. Lorriaux, F. Wallart, Apport de la
462 spectroscopie de vibration à l'approche structurale des composés de type $K_2RbLn(PO_4)_2$(Ln est
463 lanthanide), Spectrochim. Acta, Part A 52 (A) (1996) 419-427. Doi:/10.1016/0584-
464 8539(95)01575-2.

ACCEPTED MANUSCRIPT

[28] L.R. R. Nejjar, L. Benarafa, M. Saidi Idrissi, M. Knidiri, Spectres infrarouge et transition de phase par effet de pression dans les composes $K_3Lu_{1-x}Yb_x(PO_4)_2$, $Rb_3Dy(PO_4)_2$ et $K_2RbHo(PO_4)_2$, Can. J. Anal. Sci. Spectros. 43 (1998) 107-112.

[29] F.C. Hawthorne, S.V. Krivovichev, P.C. Burns, The Crystal Chemistry of Sulfate Minerals, Reviews in Mineralogy and Geochemistry 40 (2000) 1-112. Doi:10.2138/rmg.2000.40.1.

[30] SHELXTL, Siemens Analytical X-ray Instruments, Madison, WI, 1989.

[31] MDI (Materials Data Incorporated), JADE 6.0, Livermore, CA 1997.

[32] R. Shannon, Revised effective ionic radii and systematic studies of interatomic distances in halides and chalcogenides, Acta Crystallogr., Sect. A: Found. Crystallogr. 32 (1976) 751-767. Doi:10.1107/S0567739476001551.

[33]. A.C. Larson and R.B. Von Dreele, "General Structure Analysis System (GSAS)", Los Alamos National Laboratory Report LAUR 86-748 (2000).

[34]. J. Feng, B. Xiao, R. Zhou, and W. Pan, Anisotropy in elasticity and thermal conductivity of monazite-type $REPO_4$ (RE = La, Ce, Nd, Sm, Eu, and Gd) from first-principles calculations, Acta Materialia 61 (2013) 7364-7383.

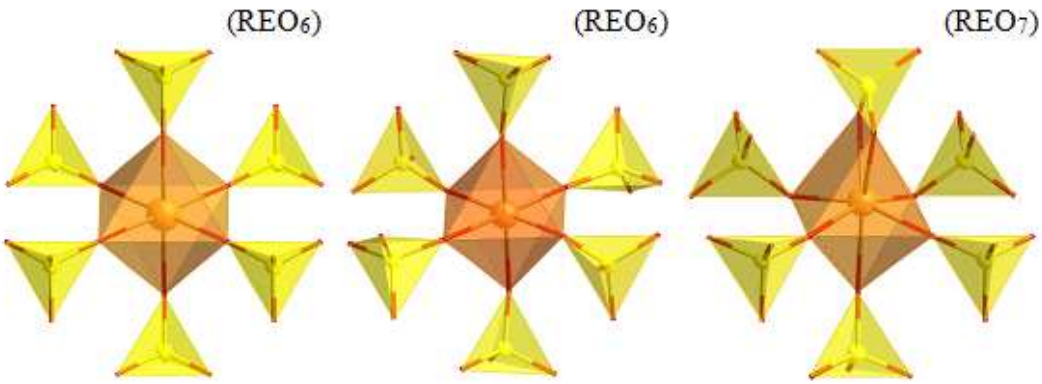

Ideal Glaserite	Distorted Glaserite	Arcanite-type
Hex. *P*-3*m*1	Hex. *P*-3	Mon. $P2_1/m$

Fig. 1. The "pinwheel"-type atomic configurations characteristic of, or related to, the glaserite structure are shown in the "ideal glaserite", "distorted glaserite", and monoclinic ("arcanite-type") forms that are under consideration here. Note that for the monoclinic distortion of the glaserite form that resembles the arcanite structure, the top phosphate group is bidentate. (After Ref. [26]).

ACCEPTED MANUSCRIPT

514

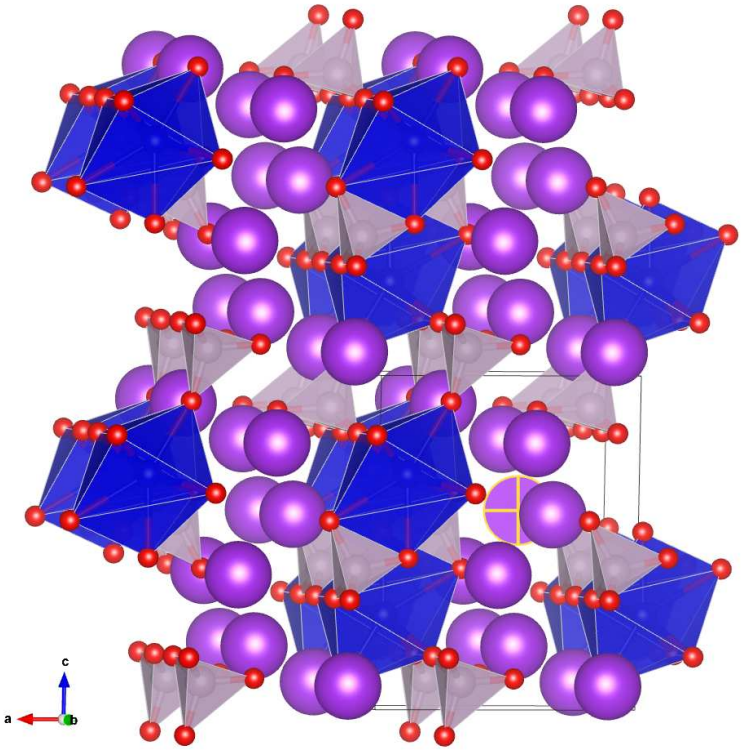

515
516 Fig. 2. The layered structure (monoclinic $P2_1/m$) of most of the $A_3RE(PO_4)_2$ compounds
517 investigated in this work. Phosphate tetrahedra are light lavender, the REO_7 polyhedron is blue,
518 and the A-site atoms are large purple balls. In this monoclinic distortion of the glaserite structure,
519 the alkali ions are located within channels of the unit cell, and one of the six PO_4 tetrahedra in
520 each "pinwheel" shares an edge with the rare-earth polyhedra.

521
522
523
524
525
526
527

528

529

ACCEPTED MANUSCRIPT

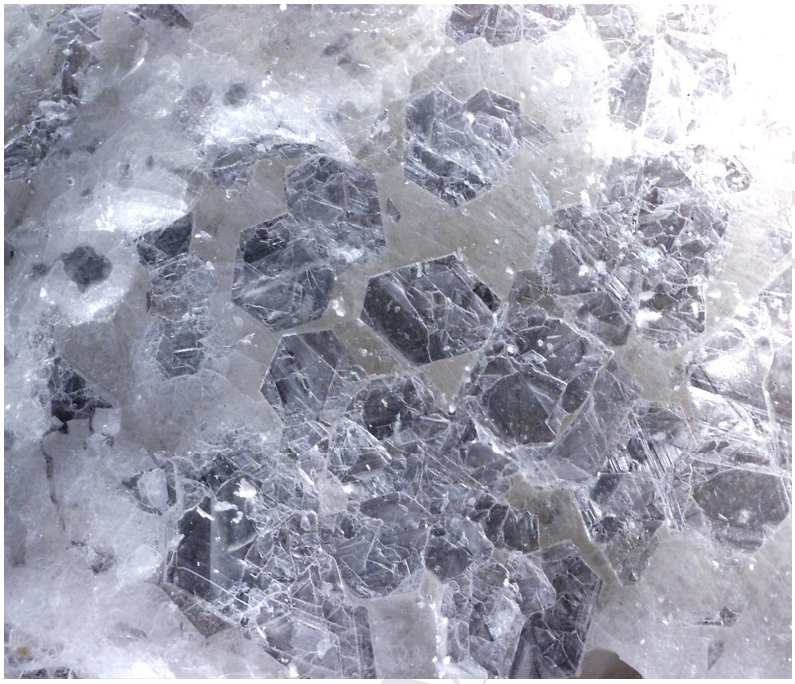

Fig. 3. Colorless single crystals of $K_3Yb(PO_4)_2$ grown as described in Section 3 illustrate the crystal growth habit, and are still entrained inside the solidified flux of the Pt crucible.

ACCEPTED MANUSCRIPT

Fig.4. Relatively large flat plates (~1.0 to 1.5 cm on a side) of clear single crystals of $K_3Lu(PO_4)_2$ are shown that were cleaved from flux-grown crystals after their removal from the growth crucible. Single crystals of this compound typically grew larger than crystals of the other alkali rare earth double phosphates.

ACCEPTED

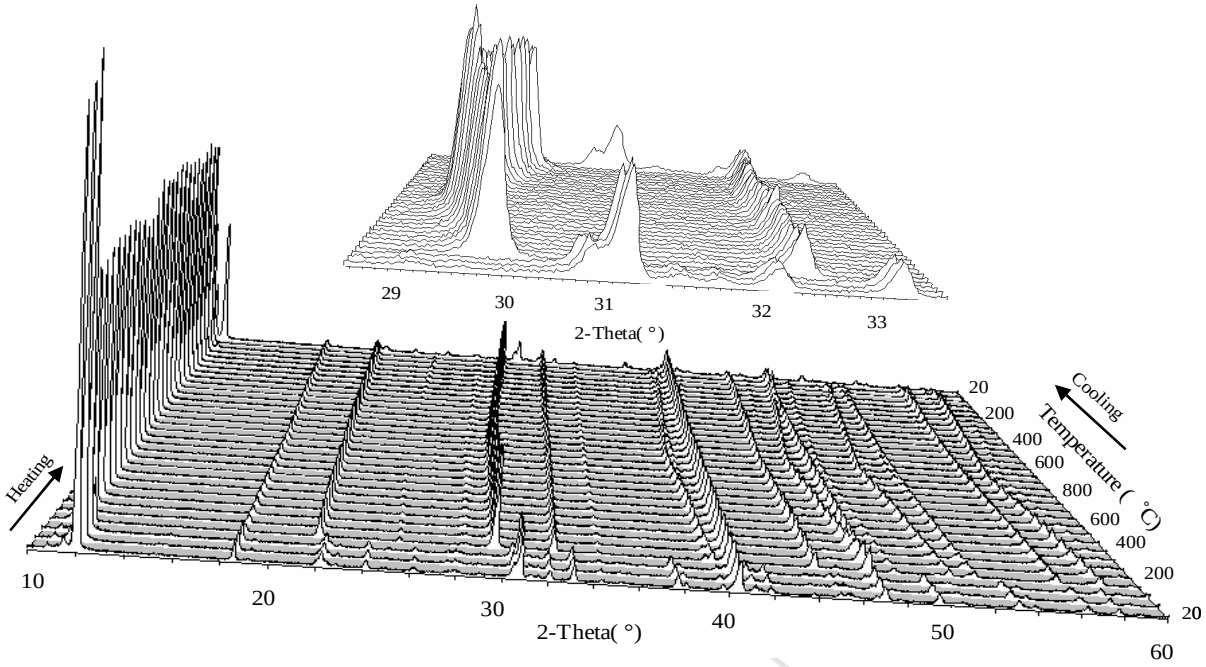

Fig. 5. High-temperature X-ray diffraction powder patterns for $K_3Yb(PO_4)_2$ for the temperature range of 20 to 800^{o}C.

ACCEPTED MANUSCRIPT

606

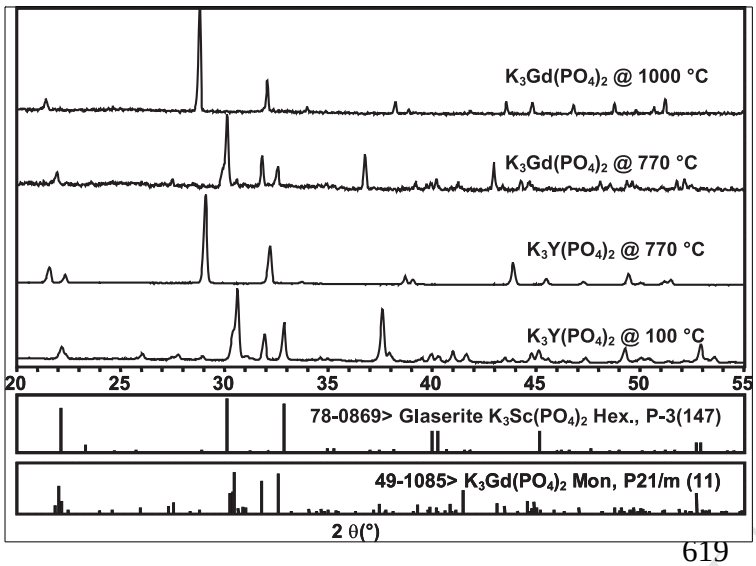

619

620

621 Fig. 6. High-temperature X-ray diffraction patterns obtained in air for $K_3Y(PO_4)_2$ and

622 $K_3Gd(PO_4)_2$. The high-temperature phases of $K_3Y(PO_4)_2$ and $K_3Gd(PO_4)_2$ are closely related to

623 the glaserite structure characteristic of $K_3Sc(PO_4)_2$ and $K_3Lu(PO_4)_2$ that is found at room

624 temperature.

625
626
627
628
629
630
631
632
633
634
635
636
637
638
639
640
641

ACCEPTED MANUSCRIPT

642

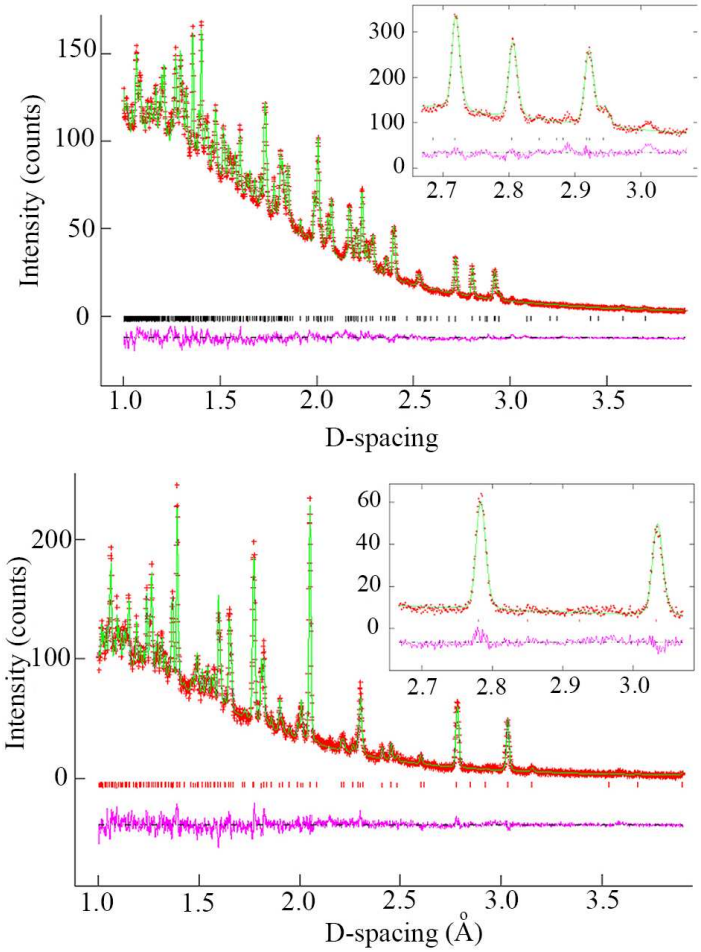

643

644 Fig. 7. The time-of-flight neutron powder diffraction pattern graphical fits from the Rietveld

645 refinement of $K_3Yb(PO_4)_2$ are shown (a –Top) for a sample temperature of 20°C and (b-Bottom)

646 a sample temperature of 200°C. A statistical summary of the results at 20 and 200°C is given in

647 Table 5.

648
649

ACCEPTED MANUSCRIPT

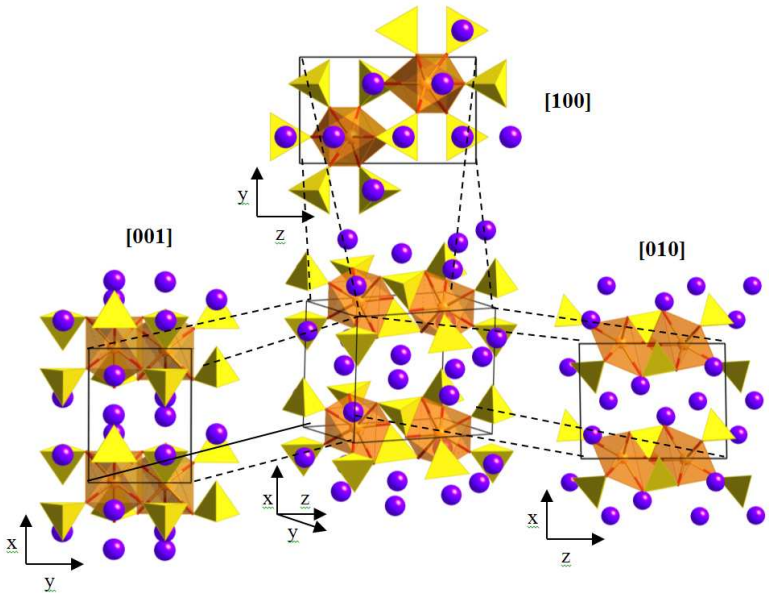

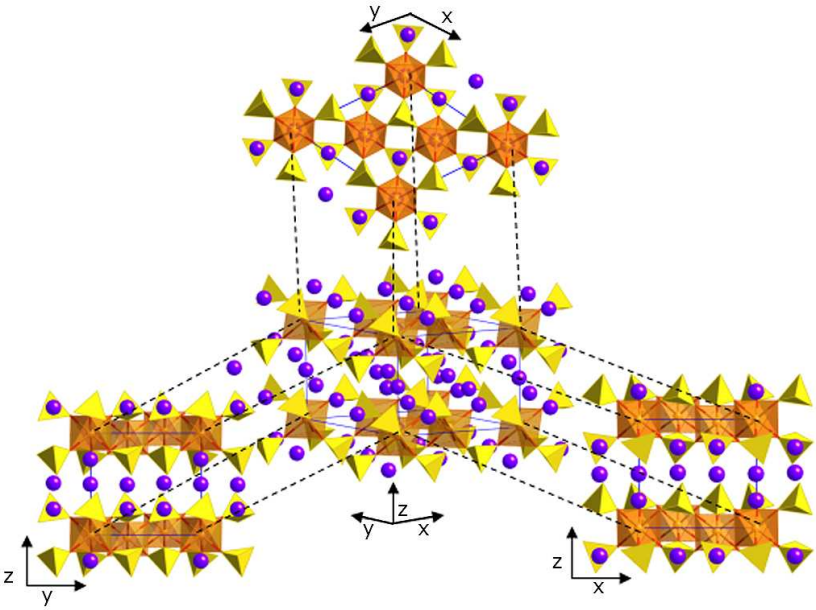

Fig. 8. Three-dimensional structural views for: (a – Top) $K_3Lu(PO_4)_2$ at room temperature[26]. The high-temperature phase of $K_3Yb(PO_4)_2$ that exists above the transition temperature of 200°C and the room-temperature phase of $K_3Lu(PO_4)_2$ are isostructural (See Table 5); and (b-Bottom) $K_3Yb(PO_4)_2$ at room temperature.

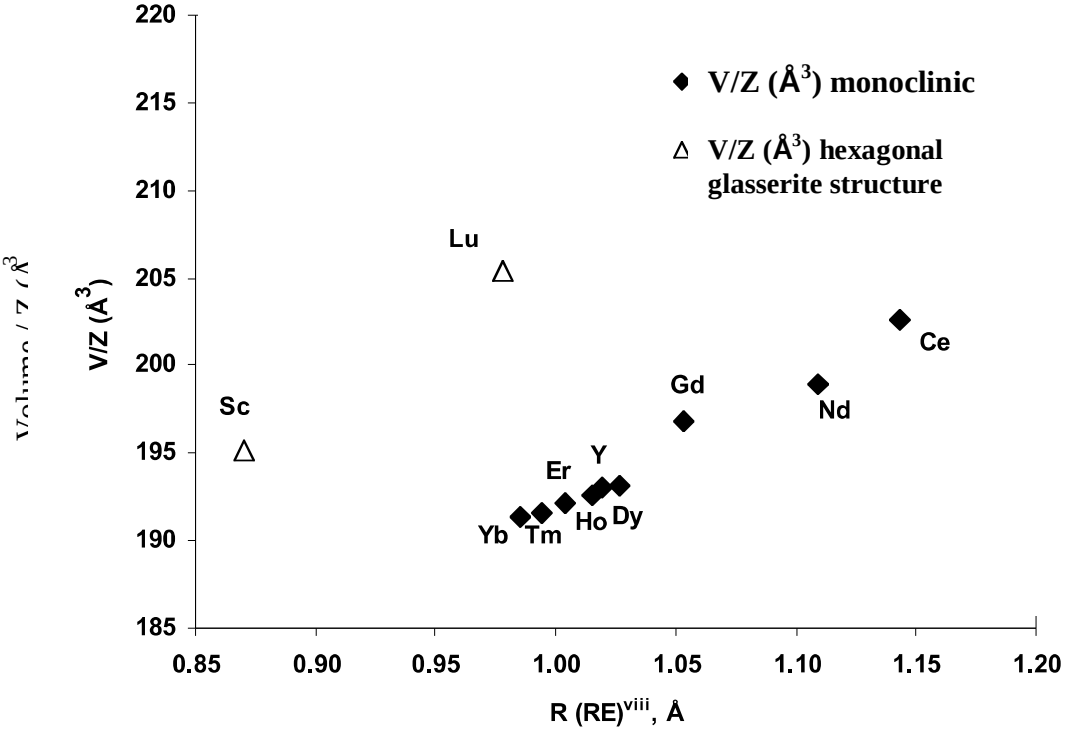

RE^{+3} radius (Å)

Fig. 9. The bond differences RE-O(1) – RE-O(2) in angstroms versus the RE^{3+} crystal radius.

ACCEPTED MANUSCRIPT

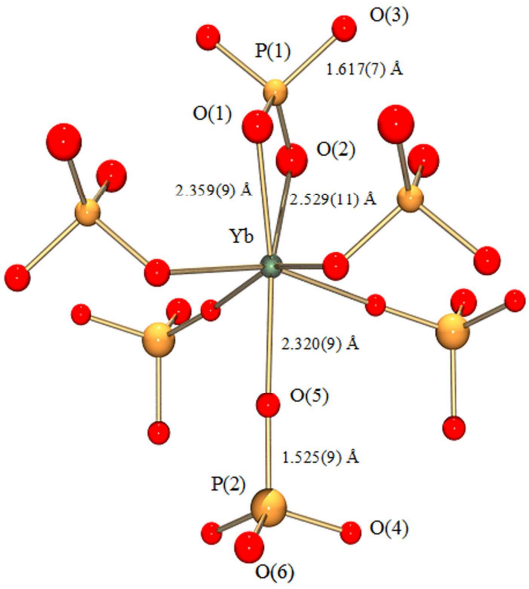

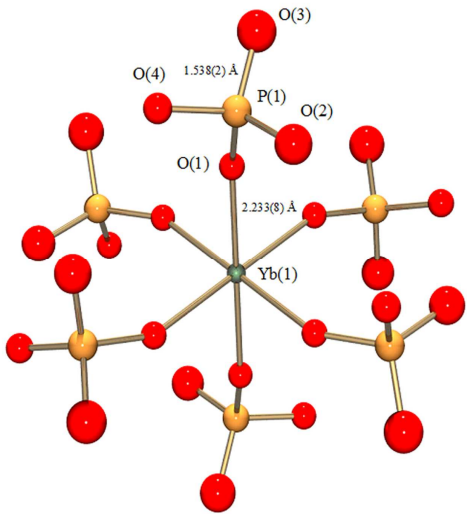

Fig. 10. (10a – Top). The room temperature complex of $K_3Yb(PO_4)_2$. The Yb ion is seven coordinated to six tetrahedrally arranged phosphate groups – one of which is bidentated; (10b – Bottom). The $K_3Yb(PO_4)_2$ complex is shown at 200°C. In this high-temperature phase of $K_3Yb(PO_4)_2$, there is a loss of the bidentation phosphate group resulting in a coordination number of six around the Yb ion and an increase in the symmetry to hexagonal P -3.

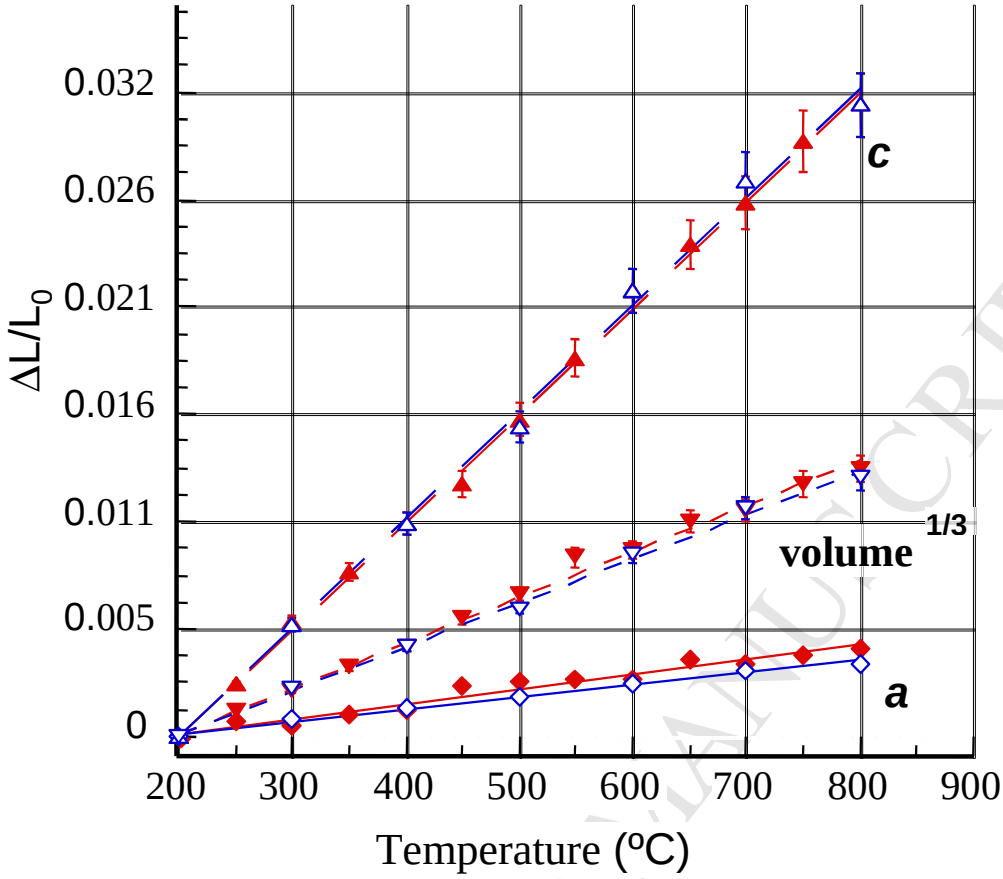

Fig. 11. $\Delta L/L_o$ versus temperature for $K_3Yb(PO_4)_2$ as determined using both high-temperature X-ray diffraction (closed symbols) and high-temperature neutron powder diffraction (open symbols).

ACCEPTED MANUSCRIPT

ACCEPTED MANUSCRIPT

Table 1. Experimental and statistical summary of several $K_3RE(PO_4)_2$ (where RE = Tm, Ho, Nd, Pr, Ce, and La)

RE	Tm	Ho	Nd	Pr	Ce	La
System	Monoclinic	Monoclinic	Monoclinic	Monoclinic	Monoclinic	Monoclinic
Space Group	$P2_1/m$	$P2_1/m$	$P2_1/m$	$P2_1/m$	$P2_1/m$	$P2_1/m$
a (Å)	7.368 (1)	7.368(1)	7.439(1)	7.458(1)	7.475(1)	7.503(1)
b (Å)	5.585(1)	5.600(1)	5.6208(1)	5.632(1)	5.648(1)	5.656(1)
c (Å)	9.311(1)	9.338(1)	9.515(1)	9.551(1)	9.601(2)	9.631(1)
β (°)	90.81(1)	90.86(1)	90.90(1)	90.87(1)	90.83(1)	90.92(1)
V (Å°)	383.11(10)	385.20(10)	397.83(10)	401.11(10)	405.26(12)	408.65(1)
Z	2	2	2	2	2	2
D_c (Mg m^{-3})	4.128	4.071	3.769	3.711	3.666	3.626
Abs. Coef. (mm^{-1})	13.641	12.321	8.511	8.043	7.565	7.16
F(000)	440	436	422	420	418	416
Delta-theta range	1.5 - 25.0	1.5 - 25.0	1.5 - 30	1.5 - 30	1.5 - 27.0	1.5 - 30
Refl collected	801	811	2447	2317	1895	2522
Indep. Reflections	742	752	1256	1253	975	1296
R_{int}	0.0629	0.0896	0.106	0.039	0.0288	0.0559
R_1	0.0399	0.0451	0.0341	0.029	0.0195	0.0412
wR_2	0.1113	0.1092	0.1154	0.0754	0.0489	0.1167
R_1 (all)	0.0422	0.0526	0.0344	0.0306	0.0213	0.0416
wR_2 (all)	0.1192	0.1136	0.1155	0.0759	0.0495	0.1169
Goodness-of-fit	1.197	1.115	1.272	1.328	1.254	1.268
Extinction coef.	0.0000(14)	0.042(6)	0.086(5)	0.0394(18)	0.090(3)	0.50(2)
Residual/(e^- A^{-3})						
min	-3.305	-3.167	-1.603	-0.986	-0.784	-1.678
max	3.294	2.814	1.189	1.268	0.587	2.395

ACCEPTED MANUSCRIPT

Table 2. Atomic coordinates and equivalent isotropic thermal coefficients (Å x 10^3) for single-crystal XRD of $K_3Tm(PO_4)_2$ at room temperature

Atom	*x*	*y*	*z*	U_{eq}
Tm	0.0078(1)	1/4	0.2869(1)	8(1)
P(1)	-0.1853(6)	1/4	0.5726(4)	8(1)
P(2)	-0.2264(6)	3/4	0.0915(4)	8(1)
O(1)	0.0159(17)	1/4	0.5356(13)	16(3)
O(2)	-0.2882(16)	1/4	0.4262(12)	13(3)
O(3)	-0.2343(11)	0.0264(15)	0.6597(8)	13(2)
O(4)	-0.1497(11)	-0.0256(16)	0.1663(9)	16(2)
O(5	-0.1698(16)	3/4	-0.0686(13)	15(3)
O(6)	-0.4313(17)	3/4	0.1025(13)	17(3)
K(1)	-0.2057(5)	1/4	-0.0802(4)	14(1)
K(2)	0.3638(5)	1/4	0.5875(4)	15(1)
K(3)	-0.4968(5)	1/4	0.1930(4)	16(1)

ACCEPTED MANUSCRIPT

ACCEPTED MANUSCRIPT

Table 3. Experimental and statistical summary for $Rb_3Lu(PO_4)_2$, $Rb_3Er(PO_4)_2$, and $K_3Sc(PO_4)_2$

Compound	$Rb_3Lu(PO_4)_2$	$Rb_3Er(PO_4)_2$	$K_3Sc(PO_4)_2$
System	Hexagonal	Hexagonal	Hexagonal
Space Group	*P*-3*m*1	*P*-3*m*1	*P*-3
a (Å)	5.622(1)	5.661(1)	9.421(1)
c (Å)	8.063(1)	8.072(1)	7.615(1)
V ($Å^3$)	220.67(7)	223.99(5)	585.32(5)
Z	1	1	3
D_c (Mg m^{-3})	4.676	4.549	2.997
Abs. Coef. (mm^{-1})	27.997	25.93	2.968
F(000)	276	273	516
Delta-theta range (˚)	1.5 - 25.0	1.5 - 25.0	1.5 - 25.0
Refl collected	428	470	1170
Indep. Reflections	171	190	680
R_{int}	0.0757	0.0823	0.0381
R_1	0.0219	0.046	0.0372
wR_2	0.0628	0.1143	0.0430
R_1 (all)	0.0235	0.0514	0.0730
wR_2 (all)	0.0645	0.1179	0.0495
Goodness-of-fit	1.166	1.110	1.101
Extinction coefficient	0.155(13)	0.044(5)	0.0048(5)
Residual/($e^- A^{-3}$)			
min	-0.838	-2.577	-0.903
max	1.58	1.279	0.595
Absorption Correction	Semi-Empirical	Semi-Empirical	Semi-Empirical

ACCEPTED MANUSCRIPT

Table 4. Atomic coordinates and equivalent isotropic atomic displacement parameters ($Å^2$ x 10^3) for single-crystal XRD $Rb_3Lu(PO_4)_2$ at room temperature

Atom	*x*	*y*	*z*	U_{eq}
Lu(1)	0	0	0	13(1)
P(1)	2/3	1/3	0.2196(4)	9(1)
O(1)	0.1847(6)	0.1847(6)	0.1561(10)	31(1)
O(2)	2/3	1/3	0.4027(14)	35(6)
Rb(1)	0	0	1/2	28(1)
Rb(2)	2/3	1/3	-0.2596(2)	15(1)

ACCEPTED MANUSCRIPT

Table 5. Summary of results for the TOF-NPD analysis of $K_3Yb(PO_4)_2$

Temperature	20˚C	200˚C
System	Monoclinic	Hexagonal
Space Group	$P2_1/m$ (No. 11)	$P\bar{3}$ (No. 147)
a (Å)	7.3972(9)	9.6340(6)
b (Å)	5.6064(8)	9.6340(6)
c (Å)	9.3183(9)	7.8017(9)
β (°)	91.00(1)	
V (Å^3)	386.42(6)	627.10(3)
Z	2	3
D_c (Mg m^{-3})	4.128	3.815
wR_p	0.032	0.071
R_p	0.024	0.051
chi	1.89	1.29
Variables	4 background	4 background
Overall	Scale factor	Scale factor
	a, b, c, and β	a and c
	Abs/refl	Abs/refl
Profile coefficients	2	2
Atomic positions	26	20
U_{iso}	12	10
Total	50	40
Number of Atoms	12	10

ACCEPTED MANUSCRIPT

ACCEPTED MANUSCRIPT

875
876 Table 6. Summary of room-temperature SXRD indexing of $A_3RE(PO_4)_2$, where RE = a rare-earth ion and A = K and Rb)
877

Compound	System	Space Group	*Z*	Cell Parameters (Å)				Volume ($Å^3$)	Density ($Mg\ m^{-3}$)
				a	*b*	*c*	β (°)		
$K_3Lu(PO_4)_2$[a]	Hexagonal	*P*-3 (No. 147)	3	9.606 (1)	9.606 (1)	7.711(2)		616.20(10)	4.238
$K_3Yb(PO_4)_2$	Monoclinic	$P2_1/m$ (No. 11)	2	7.372(1)	5.589(1)	9.292(2)	91.03(3)	382.81(11)	4.167
$K_3Tm(PO_4)_2$	Monoclinic	$P2_1/m$ (No. 11)	2	7.368(1)	5.585(1)	9.311(1)	90.81(1)	383.11(10)	4.128
$K_3Er(PO_4)_2$	Monoclinic	$P2_1/m$ (No. 11)	2	7.371(1)	5.595(1)	9.318(1)	90.90(1)	384.23(11)	4.101
$K_3Ho(PO_4)_2$	Monoclinic	$P2_1/m$ (No. 11)	2	7.367(1)	5.600(1)	9.338(1)	90.86(1)	385.20(10)	4.071
$K_3Dy(PO_4)_2$	Monoclinic	$P2_1/m$ (No. 11)	2	7.373(1)	5.602(1)	9.352(1)	90.88(1)	386.22(11)	4.039
$K_3Tb(PO_4)_2$	Monoclinic	$P2_1/m$ (No. 11)	2	7.390(2)	5.603(1)	9.396(1)	90.87(1)	389.01(10)	3.979
$K_3Gd(PO_4)_2$	Monoclinic	$P2_1/m$ (No. 11)	2	7.415(1)	5.625(1)	9.436(1)	90.88(1)	393.58(11)	3.919
$K_3Eu(PO_4)_2$	Monoclinic	$P2_1/m$ (No. 11)	2	7.423(2)	5.624(1)	9.443(1)	90.90(1)	394.17(11)	3.869
$K_3Sm(PO_4)_2$	Monoclinic	$P2_1/m$ (No. 11)	2	7.430(1)	5.622(1)	9.478(1)	90.89(1)	395.86(10)	3.839
$K_3Nd(PO_4)_2$	Monoclinic	$P2_1/m$ (No. 11)	2	7.439(1)	5.621(1)	9.515(1)	90.90(1)	397.83(10)	3.769
$K_3Pr(PO_4)_2$	Monoclinic	$P2_1/m$ (No. 11)	2	7.458(1)	5.632(1)	9.551(1)	90.87(1)	401.11(10)	3.711
$K_3Ce(PO_4)_2$	Monoclinic	$P2_1/m$ (No. 11)	2	7.475(1)	5.648(1)	9.601(2)	90.83(1)	405.26(12)	3.666
$K_3La(PO_4)_2$	Monoclinic	$P2_1/m$ (No. 11)	2	7.503(1)	5.656(1)	9.631(1)	90.92(1)	408.65(1)	3.626
$K_3Y(PO_4)_2$	Monoclinic	$P2_1/m$ (No. 11)	2	7.358(1)	5.613(1)	9.349(1)	90.92(1)	386.12(7)	3.407
$K_3Sc(PO_4)_2$	Hexagonal	*P*-3 (No. 147)	3	9.421(1)	9.421(1)	7.615(1)		585.34(10)	2.997
$Rb_3Lu(PO_4)_2$	Hexagonal	*P*-3*m*1 (No. 164)	1	5.622(1)	5.622(1)	8.063(1)		220.67(10)	4.676
$Rb_3Er(PO_4)_2$	Hexagonal	*P*-3*m*1 (No. 164)	1	5.661(1)	5.661(1)	8.072(1)		223.99(5)	4.549

ACCEPTED MANUSCRIPT

878 Table 7. $K_3RE(PO_4)_2$ bond distances (Å) (where RE = Lu, Yb, Tm, Ho, Nd, Pr, Ce, and La)

distance	Lu[a]	Yb[b]	Tm	Ho	Nd	Pr	Ce	La
RE-O(1)	2.282(12)	2.305(9)	2.315(12)	2.370(11)	2.494(9)	2.530(7)	2.559(5)	2.575(9)
RE-O(2)	2.567(13)	2.607(11)	2.554(12)	2.504(11)	2.531(7)	2.549(6)	2.558(4)	2.559(7)
RE-O(3)$_{ii}$ × 2	2.290(9)	2.308(7)	2.322(8)	2.339(7)	2.444(5)	2.469(4)	2.485(3)	2.510(5)
RE-O(4) × 2	2.215(9)	2.213(7)	2.22(9)	2.247(8)	2.334(5)	2.353(4)	2.367(3)	2.387(5)
RE-O(5)$_{iv}$	2.373(14)	2.380(10)	2.372(12)	2.405(11)	2.483(7)	2.495(5)	2.511(3)	2.531(7)
P(1)-O(1)	1.532(13)	1.519(12)	1.527(13)	1.522(12)	1.528(8)	1.530(7)	1.525(4)	1.535(8)
P(1)-O(2)	1.554(13)	1.536(9)	1.551(11)	1.545(11)	1.530(7)	1.551(5)	1.548(4)	1.551(7)
P(1)-O(3) × 2	1.549(10)	1.550(6)	1.535(18)	1.546(8)	1.535(5)	1.542(4)	1.535(3)	1.530(6)
P(2)-O(4) × 2	1.531(9)	1.537(6)	1.538(9)	1.541(8)	1.547(5)	1.543(4)	1.549(3)	1.550(5)
P(2)-O(5)	1.518(14)	1.533(9)	1.553(13)	1.530(12)	1.537(7)	1.545(5)	1.545(4)	1.541(7)
P(2)-O(6)	1.523(13)	1.537(6)	1.515(13)	1.537(12)	1.513(7)	1.507(6)	1.511(4)	1.523(7)

879 [a] at 100 K in this study; [b] from Farmer; [ii] –x,y + ½, -z +1; [iv] –x, -y, -z

880
881
882
883
884
885
886
887
888
889
890

ACCEPTED MANUSCRIPT

ACCEPTED MANUSCRIPT

891 Table 8. $K_3RE(PO_4)_2$ phosphate tetrahedral angles (˚) (where RE = Lu, Yb, Tm, Ho, Nd, Pr, Ce, and La)

Angle	Lu[a]	Yb[b]	Tm	Ho	Nd	Pr	Ce	La
O(1)-P(1)-O(2)	105.3(7)	106.2(6)	105.4(7)	105.5(6)	106.2(4)	107.1(3)	107.3(2)	106.7(4)
O(1)-P(1)-O(3)	110.6(5)	111.4(3)	110.8(4)	110.5(4)	110.0(3)	110.2(2)	109.7(1)	109.7(3)
O(2)-P(1)-O(3)	111.2(4)	109.9(3)	110.4(4)	110.7(4)	110.7(2)	110.0(2)	110.2(1)	110.4(3)
$O(3)-P(1)-O(3)_i$	108.1(7)	108.1(5)	108.9(7)	108.9(6)	109.2(4)	109.4(3)	109.8(8)	109.9(4)
O(4)-P(2)-O(5)	109.8(5)	109.2(4)	109.5(4)	109.8(4)	108.6(2)	108.9(2)	108.7(1)	108.6(2)
O(4)-P(2)-O(6)	108.3(5)	108.9(4)	109.2(4)	108.3(4)	109.2(3)	109.4(2)	109.4(1)	109.2(3)
O(5)-P(2)-O(6)	111.0(7)	111.6(6)	110.3(7)	111.0(7)	112.0(4)	111.4(3)	111.8(2)	112.1(4)
$O(4)-P(2)-O(4)_v$	109.5(7)	109.0(5)	109.2(7)	109.4(6)	109.3(4)	108.8(3)	108.8(2)	109.1(4)

892 [a] at 100 K in this study; [b] from Farmer; [i] x, -y + ½, z; [v] x,-y – ½, z

ACCEPTED MANUSCRIPT

ACCEPTED MANUSCRIPT

Table 9. RE-O(1) - RE-O(2) bond difference (Å) for $K_3RE(PO_4)_2$ (where RE = Lu, Yb, Tm, Ho, Nd, Pr, Ce, and La)

RE	RE-O(1) - RE-O(2) bond difference
Lu	0.285 (12)
Yb[a]	0.302(10)
Tm	0.239 (12)
Ho	0.134 (11)
Nd	0.037 (8)
Pr	0.019 (6)
Ce	-0.001 (4)
La	-0.016 (6)

[a] at 100 K

ACCEPTED MANUSCRIPT

898 Table 10. $Rb_3Lu(PO_4)_2$ and $Rb_3Er(PO_4)_2$ bond distances (Å)

Bond	$Rb_3Lu(PO_4)_2$	$Rb_3Er(PO_4)_2$
RE-O(1) x 6	2.195(6)	2.236(7)
P(1)-O(1) x 2	1.535(6)	1.528(6)
P(1)-O(2) x 2	1.476(13)	1.463(14)

899
900
901 $Rb_3Lu(PO_4)_2$ and $Rb_3Er(PO_4)_2$ phosphate tetrahedral angles (˚)

Angle	$Rb_3Lu(PO_4)_2$	$Rb_3Er(PO_4)_2$
O(1)P(1)-O(2)	109.5(3)	109.0(4)
$O(1)\text{-}P(1)\text{-}O(1)_{xviii}$	109.5(3)	110.0(4)
$O(2)\text{-}P(1)\text{-}O(1)_{xviii}$	109.5(3)	109.0(4)
$O(1)\text{-}P(1)\text{-}O(1)_{xix}$	109.5(3)	110.0(4)

902 [xvii] –x + y – 1, -x, z; [xix] –y, x- y + 1, z

903
904 $Rb_3Lu(PO_4)_2$ and $Rb_3Er(PO_4)_2$ phosphate angles (˚)

Angle	$Rb_3Lu(PO_4)_2$	$Rb_3Er(PO_4)_2$
O(1)P(1)-O(2)	109.5(3)	109.0(4)
$O(1)\text{-}P(1)\text{-}O(1)_{xviii}$	109.5(3)	110.0(4)
$O(2)\text{-}P(1)\text{-}O(1)_{xviii}$	109.5(3)	109.0(4)
$O(1)\text{-}P(1)\text{-}O(1)_{xix}$	109.5(3)	110.0(4)

905 [xvii] –x + y – 1, -x, z; [xix] –y, x- y + 1, z

906
907
908
909

ACCEPTED MANUSCRIPT

910 Table 11. Thermal expansion ($^{\circ}C^{-1}$) of $K_3Yb(PO_4)_2$ calculated using X-ray and Neutron powder
911 diffraction
912

	$K_3Yb(PO_4)_2$	
α	TOF-NPD	HTXRD
α_a	6.01	7.26
α_c	53.1	52.8
$\alpha V^{1/3}$	21.5	22.5
α_c / α_a	8.82	7.27

913
914

915

ACCEPTED MANUSCRIPT

ACCEPTED MANUSCRIPT

APPENDIX A

Atomic Coordinates and Equivalent Isotropic Atomic Displacement Parameters

Table A1. Atomic coordinates and equivalent isotropic atomic displacement parameters ($Å^2$ x 10^3) for single-crystal XRD of $K_3Ho(PO_4)_2$ at room temperature

Atom	*x*	*y*	*z*	U_{eq}
Ho	0.0074(1)	1/4	0.2883(1)	16(1)
P(1)	-0.1858(5)	1/4	0.5733(4)	17(1)
P(2)	-0.2274(5)	3/4	0.0893(4)	16(1)
O(1)	0.0164(15)	1/4	0.5420(12)	22(2)
O(2)	-0.2822(15)	1/4	0.4252(12)	22(2)
O(3)	-0.2377(10)	0.0255(14)	0.6597(8)	19(2)
O(4)	-0.1516(10)	-0.0255(14)	0.1645(8)	21(2)
O(5)	-0.1727(15)	3/4	-0.0682(12)	21(2)
O(6)	-0.4350(15)	3/4	0.1034(13)	25(3)
K(1)	-0.2050(5)	1/4	-0.0808(4)	23(1)
K(2)	0.3652(5)	1/4	0.5888(4)	24(1)
K(3)	-0.4967(5)	1/4	0.1927(4)	24(1)

ACCEPTED MANUSCRIPT

Table A2. Atomic coordinates and equivalent isotropic atomic displacement parameters ($Å^2$ x 10^3) for single-crystal XRD of $K_3Tm(PO_4)_2$ at room temperature

Atom	*x*	*y*	*z*	U_{eq}
Nd	0.0078(1)	1/4	0.2913(1)	8(1)
P(1)	-0.1970(3)	1/4	0.5742(2)	12(1)
P(2)	-0.2346(3)	3/4	0.0857(2)	9(1)
O(1)	0.0063(11)	1/4	0.5534(9)	57(5)
O(2)	-0.2823(9)	1/4	0.4268(7)	12(1)
O(3)	-0.2527(7)	0.0274(10)	0.6562(5)	20(1)
O(4)	-0.1561(7)	-0.0256(9)	0.1579(5)	17(1)
O(5)	-0.1782(10)	3/4	-0.0690(7)	17(1)
O(6)	-0.4368(9)	3/4	0.1003(8)	19(1)
K(1)	-0.2045(3)	1/4	-0.0824(2)	18(1)
K(2)	0.3623(3)	1/4	0.5935(2)	18(1)
K(3)	-0.4919(3)	1/4	0.1911(2)	17(1)

Table A3. Atomic coordinates and equivalent isotropic atomic displacement parameters ($Å^2$ x 10^3) for single-crystal XRD of $K_3Pr(PO_4)_2$ at room temperature

Atom	*x*	*y*	*z*	U_{eq}
Pr	0.0080(1)	1/4	0.2915(1)	8(1)
P(1)	-0.1984(3)	1/4	0.5745(2)	12(1)
P(2)	-0.2355(3)	3/4	0.0856(2)	9(1)
O(1)	0.0052(9)	1/4	0.5564(7)	53(3)
O(2)	-0.2847(7)	1/4	0.4257(5)	12(1)
O(3)	-0.2567(6)	0.0265(8)	0.6553(4)	19(1)
O(4)	-0.1569(6)	-0.0273(7)	0.1579(4)	18(1)
O(5)	-0.1804(8)	3/4	-0.0697(5)	15(1)
O(6)	-0.4364(8)	3/4	0.0997(6)	18(1)
K(1)	-0.2042(3)	1/4	-0.0826(2)	17(1)
K(2)	0.3618(2)	1/4	0.5941(2)	18(1)
K(3)	-0.4919(2)	1/4	0.1914(2)	17(1)

Table A4. Atomic coordinates and equivalent isotropic atomic displacement parameters ($Å^2$ x 10^3) for single-crystal XRD of $K_3Ce(PO_4)_2$ at room temperature

Atom	*x*	*y*	*z*	U_{eq}
Ce	0.0084(1)	1/4	0.2917(1)	8(1)
P(1)	-0.2003(2)	1/4	0.5743(1)	10(1)
P(2)	-0.2362(2)	3/4	0.0853(1)	7(1)
O(1)	0.0024(6)	1/4	0.5581(5)	40(2)
O(2)	-0.2845(5)	1/4	0.4261(4)	10(1)
O(3)	-0.2578(4)	0.0276(5)	0.6540(3)	17(1)
O(4)	-0.1571(4)	-0.0270(5)	0.1571(3)	16(1)
O(5)	-0.1803(5)	3/4	-0.0689(4)	14(1)
O(6)	-0.4372(5)	3/4	0.0999(4)	19(1)
K(1)	-0.2041(2)	1/4	-0.0832(1)	15(1)
K(2)	0.3612(2)	1/4	0.5946(1)	17(1)
K(3)	-0.4917(2)	1/4	0.1915(1)	16(1)

Table A5. Atomic coordinates and equivalent isotropic atomic displacement parameters ($Å^2$ x 10^3) for single-crystal XRD of $K_3La(PO_4)_2$ at room temperature

Atom	*x*	*y*	*z*	U_{eq}
La	0.0087(1)	1/4	0.2924(1)	12(1)
P(1)	-0.2031(3)	1/4	0.5746(2)	16(1)
P(2)	-0.2371(3)	3/4	0.0844(2)	11(1)
O(1)	0.0003(10)	1/4	0.5595(9)	57(4)
O(2)	-0.2838(9)	1/4	0.4254(7)	16(1)
O(3)	-0.2608(7)	0.0284(10)	0.6532(5)	23(1)
O(4)	-0.1585(7)	-0.0268(10)	0.1559(5)	21(1)
O(5)	-0.1817(9)	3/4	-0.0689(7)	17(1)
O(6)	-0.4388(9)	3/4	0.0998(8)	22(2)
K(1)	-0.2045(3)	1/4	-.0830(2)	19(1)
K(2)	0.3608(3)	1/4	0.5959(2)	22(1)
K(3)	-0.4910(3)	1/4	0.1911(2)	20(1)

ACCEPTED MANUSCRIPT

Table A6. Atomic coordinates and equivalent isotropic atomic displacement parameters ($Å^2$ x 10^3) for single-crystal XRD of $K_3Sc(PO_4)_2$ at room temperature

Atom	*x*	*y*	*z*	U_{eq}
Sc(1)	0	0	0	8(1)
Sc(2)	2/3	1/3	-0.0284(2)	7(1)
P(1)	0.3398(3)	0.0113(2)	0.2243(1)	7(1)
O(1)	0.3625(7)	0.0599(5)	0.4147(4)	28(1)
O(2)	0.1774(6)	-0.0053(5)	0.1605(8)	19(1)
O(3)	0.3335(6)	-0.1536(5)	0.1971(5)	13(1)
O(4)	0.4823(5)	0.1443(5)	0.1168(5)	20(1)
K(1)	0	0	1/2	34(1)
K(2)	2/3	1/3	0.4945(3)	21(1)
K(3)	0.3336(2)	-0.0013(1)	-0.2496(1)	16(1)

Table A7. Atomic coordinates and equivalent isotropic atomic displacement parameters ($Å^2$ x 10^3) for single crystal XRD $Rb_3Er(PO_4)_2$ at room temperature

Atom	*x*	*y*	*z*	U_{eq}
Er	0	0	0	12(1)
P(1)	2/3	1/3	0.2219(5)	8(1)
O(1)	0.1859(6)	0.1859(6)	0.1604(11)	31(2)
O(2)	2/3	1/3	0.4032(17)	72(6)
Rb(1)	0	0	1/2	28(1)
Rb(2)	2/3	1/3	-0.2585(2)	13(1)

ACCEPTED MANUSCRIPT

ACCEPTED MANUSCRIPT

APPENDIX B

Tables of Anisotropic Atomic Displacement Parameters – U's

Table B1. Anisotropic ADPs (Å x 10^3) for single-crystal XRD of $K_3Sc(PO_4)_2$ at room temperature

Atom	*U*(11)	*U*(22)	*U*(33)	*U*(23)	*U*(13)	*U*(12)
Sc(1)	6(1)	6(1)	12(2)	0	0	3(1)
Sc(2)	5(1)	5(1)	10(1)	0	0	3(1)
P(1)	7(1)	6(1)	9(1)	-1(1)	1(1)	3(1)
O(1)	45(3)	23(2)	14(2)	-7(2)	-7(2)	16(3)
O(2)	10(2)	7(3)	38(3)	0(2)	-7(2)	4(2)
O(3)	14(2)	9(2)	18(2)	-4(2)	-1(2)	8(2)
O(4)	18(3)	12(2)	30(2)	9(2)	8(2)	7(2)
K(1)	40(2)	40(2)	20(3)	0	0	20(1)
K(2)	23(1)	23(1)	16(1)	0	0	11(1)
K(3)	12(1)	13(1)	23(1)	-1(1)	-2(1)	6(1)

ACCEPTED MANUSCRIPT

Table B2. Anisotropic ADPs (Å x 10^3) for single-crystal XRD of $K_3Tm(PO_4)_2$ at room temperature

Atom	*U*(11)	*U*(22)	*U*(33)	*U*(12)	*U*(13)	*U*(23)
Tm	11(1)	5(1)	9(1)	0	-3(1)	0
P(1)	11(2)	4(2)	9(2)	0	-2(2)	0
P(2)	10(2)	6(2)	9(2)	0	-1(2)	0
O(1)	19(7)	17(6)	13(6)	0	1(5)	0
O(2)	16(6)	10(6)	12(6)	0	-12(5)	0
O(3)	19(4)	8(4)	11(4)	-1(3)	-1(3)	2(4)
O(4)	14(4)	14(4)	19(4)	1(4)	-4(3)	-3(4)
O(5)	11(6)	19(6)	17(6)	0	-1(5)	0
O(6)	18(6)	20(7)	15(6)	0	0(5)	0
K(1)	21(2)	9(2)	12(2)	0	-1(1)	0
K(2)	16(2)	14(2)	16(2)	0	-3(1)	0
K(3)	15(2)	18(2)	14(2)	0	-5(1)	0

Table B3. Anisotropic ADPs (Å x 10^3) for single-crystal XRD of $K_3Ho(PO_4)_2$ at room temperature

Atom	*U*(11)	*U*(22)	*U*(33)	*U*(12)	*U*(13)	*U*(23)
Ho	18(1)	12(1)	20(1)	0	-1(1)	0
P(1)	22(2)	9(2)	19(2)	0	0(2)	0
P(2)	20(2)	9(2)	20(2)	0	-1(2)	0
O(1)	21(6)	21(6)	25(6)	0	-4(5)	0
O(2)	29(6)	19(6)	19(6)	0	3(5)	0
O(3)	23(4)	12(4)	23(4)	3(3)	0(3)	0(3)
O(4)	24(4)	16(4)	23(4)	1(3)	-1(3)	-3(3)
O(5)	21(6)	16(6)	26(6)	0	5(5)	0
O(6)	21(6)	21(6)	32(6)	0	2(5)	0
K(1)	29(2)	16(2)	25(2)	0	-1(1)	0
K(2)	24(2)	18(2)	29(2)	0	2(1)	0
K(3)	24(2)	24(2)	25(2)	0	-3(1)	0

ACCEPTED MANUSCRIPT

Table B4. Anisotropic ADPs (Å x 10^3) for single-crystal XRD of $K_3Pr(PO_4)_2$ at room temperature

Atom	*U*(11)	*U*(22)	*U*(33)	*U*(12)	*U*(13)	*U*(23)
Pr	8(1)	9(1)	8(1)	0	-1(1)	0
P(1)	7(1)	21(1)	9(1)	0	-2(1)	0
P(2)	9(1)	9(1)	8(1)	0	-1(1)	0
O(1)	9(3)	137(10)	14(3)	0	-2(2)	0
O(2)	14(2)	14(2)	8(2)	0	-5(2)	0
O(3)	23(2)	21(2)	14(2)	3(2)	1(2)	9(2)
O(4)	24(2)	13(2)	15(2)	-3(1)	-2(1)	-6(2)
O(5)	14(3)	24(3)	7(2)	0	2(2)	0
O(6)	11(2)	26(3)	18(3)	0	0(2)	0
K(1)	21(1)	16(1)	15(1)	0	0(1)	0
K(2)	13(1)	23(1)	17(1)	0	-2(1)	0
K(3)	14(1)	24(1)	14(1)	0	-3(1)	0

Table B5. Anisotropic ADPs (Å x 10^3) for single-crystal XRD of $K_3Nd(PO_4)_2$ at room temperature

Atom	*U*(11)	*U*(22)	*U*(33)	*U*(12)	*U*(13)	*U*(23)
Nd	9(1)	8(1)	8(1)	0	0(1)	0
P(1)	9(1)	21(1)	7(1)	0	0(1)	0
P(2)	10(1)	7(1)	9(1)	0	1(1)	0
O(1)	11(3)	148(15)	12(3)	0	-1(3)	0
O(2)	15(3)	16(3)	6(3)	0	-3(2)	0
O(3)	30(2)	18(2)	12(2)	5(2)	3(2)	13(3)
O(4)	26(2)	12(2)	14(2)	-2(2)	0(2)	-5(2)
O(5)	15(3)	28(4)	8(3)	0	1(2)	0
O(6)	11(3)	22(4)	24(3)	0	-3(3)	0
K(1)	23(1)	15(1)	16(1)	0	1(1)	0
K(2)	14(1)	22(1)	18(1)	0	-1(1)	0
K(3)	14(1)	23(1)	14(1)	0	-2(1)	0

ACCEPTED MANUSCRIPT

Table B6. Anisotropic ADPs (Å x 10^3) for single-crystal XRD of $K_3Tm(PO_4)_2$ at room temperature

Atom	*U*(11)	*U*(22)	*U*(33)	*U*(12)	*U*(13)	*U*(23)
La	13(1)	11(1)	11(1)	0	-3(1)	0
P(1)	13(1)	23(1)	11(1)	0	-4(1)	0
P(2)	13(1)	10(1)	11(1)	0	-3(1)	0
O(1)	10(3)	140(14)	19(4)	0	-4(3)	0
O(2)	20(3)	18(3)	10(3)	0	-5(2)	0
O(3)	31(2)	22(2)	15(2)	4(2)	1(2)	12(2)
O(4)	30(2)	13(2)	18(2)	-3(2)	-4(2)	-7(2)
O(5)	18(3)	22(4)	11(3)	0	-1(2)	0
O(6)	15(3)	27(4)	24(3)	0	-5(3)	0
K(1)	24(1)	14(1)	17(1)	0	-3(1)	0
K(2)	19(1)	25(1)	22(1)	0	-4(1)	0
K(3)	17(1)	24(1)	18(1)	0	-5(1)	0

Table B7. Anisotropic ADPs (Å x 10^3) for single-crystal XRD of $K_3Ce(PO_4)_2$ at room temperature

Atom	*U*(11)	*U*(22)	*U*(33)	*U*(12)	*U*(13)	*U*(23)
Ce	8(1)	9(1)	7(1)	0	0(1)	0
P(1)	8(1)	16(1)	7(1)	0	0(1)	0
P(2)	8(1)	8(1)	6(1)	0	0(1)	0
O(1)	9(2)	96(5)	16(2)	0	1(2)	0
O(2)	13(2)	11(2)	7(2)	0	-2(1)	0
O(3)	23(1)	15(1)	13(1)	4(1)	3(1)	7(1)
O(4)	21(1)	13(1)	14(1)	-4(1)	-2(1)	-4(1)
O(5)	14(2)	21(2)	6(2)	0	2(1)	0
O(6)	10(2)	29(2)	18(2)	0	0(2)	0
K(1)	19(1)	13(1)	13(1)	0	2(1)	0
K(2)	15(1)	20(1)	16(1)	0	-1(1)	0
K(3)	12(1)	23(1)	13(1)	0	-2(1)	0

ACCEPTED MANUSCRIPT

Table B8. Anisotropic ADPs (Å x 10^3) for single-crystal XRD of $Rb_3Lu(PO_4)_2$ at room temperature

Atom	*U*(11)	*U*(22)	*U*(33)	*U*(23)	*U*(13)	*U*(12)
Lu	6(1)	6(1)	26(1)	0	0	3(1)
P	10(1)	10(1)	7(2)	0	0	5(1)
O(1)	13(2)	13(2)	66(4)	-6(2)	6(2)	7(2)
O(2)	107(10)	107(10)	12(5)	0	0	53(5)
Rb(1)	33(1)	33(1)	19(1)	0	0	17(1)
Rb(2)	12(1)	12(1)	21(1)	0	0	6(1)

Table B9. Anisotropic ADPs (Å x 10^3) for single-crystal XRD of $Rb_3Er(PO_4)_2$ at room temperature

Atom	*U*(11)	*U*(22)	*U*(33)	*U*(23)	*U*(13)	*U*(12)
Er	5(1)	5(1)	26(1)	0	0	2(1)
P	8(1)	8(1)	9(2)	0	0	4(1)
O(1)	11(2)	11(2)	72(5)	-7(2)	7(2)	5(3)
O(2)	102(9)	102(9)	12(7)	0	0	51(5)
Rb(1)	34(1)	34(1)	15(1)	0	0	17(1)
Rb(2)	11(1)	11(1)	18(1)	0	0	5(1)

ACCEPTED MANUSCRIPT

ACCEPTED MANUSCRIPT

Structural and Crystal Chemical Properties of Alkali Rare-earth Double Phosphates

J. Matt Farmer[1], L. A. Boatner[1,2a], Bryan C. Chakoumakos[3], and Claudia J. Rawn[1]

HIGHLIGHTS:

- Comprehensive structural data obtained for alkali rare-earth double phosphates
- New structural phase transition discovered for alkali rare-earth double phosphates
- Fundamental properties of RE double phosphates for future scintillator research

ACCEPTED MANUSCRIPT